cea liten

CONFIDENTIAL

Technical Report DEHT/LV/2023/114

MEASUREMENT AND MODELLING OF PROTON AND OXYGEN TRANSPORT LIMITATIONS IN PEMFC ELECTRODES

Author (s) : Anjali YADAV

Project reference	P19-00737
Project title	FURTHER-FC
Project duration	06/03/2023 – 08/08/2023
Nature of the report	❑ Progress Report ❑ Final Report ❑ Contribution to a global report ❑ Work package report (WP) ☒Others : non included on the agreement
Appendices (to complete inevitably for « Restricted Distribution)	❑ YES ☒NO If the report include appendices, specify : Appendices XX from page XXX to page XXX

	Writer(s)	Controller	Approver	Transmitter
Name(s)	Anjali Yadav	Arnaud Morin Pascal Schott Philippe Clément	Béatrice Icard	Véronique Carron
Position	Intern	Project Leader & Head of laboratory or expert	Head of Service	Head of Department
Date	26/07/2023			

Liten
Laboratoire d'Innovation pour les Technologies des Energies Nouvelles et les nanomatériaux
Commissariat à l'énergie atomique et aux énergies alternatives
17 rue des Martyrs
38054 Cedex 9
T. +33 (0)4 38 78 20 00 | F. +33 (0)4 38 78 25 56
Marie-laure.BENTIVOGLIO@cea.fr

Direction de la Recherche Technologique
Département : DEHT
Service : STP
Laboratoire : LCP

FOLLOW-UP OF THE REVISIONS

Index	Date	Cause and description of the modification
A	26/07/2023	Initial Document

EXTERNAL DISTRIBUTION

CUSTOMER	Enter the name, first name and email address of the recipients at the customer

INTERNAL DISTRIBUTION

LITEN	F. LEGALLAND, Head of LITEN B. CASSINI, Deputy Director of Operations Financial Office
DEPARTMENT DEHT	Mme Véronique Carron Programs Correspondent Mme Marie-Laure Bentivoglio
SERVICE AND LABORATORY STP/LCP	Mme Béatrice Icard M. Philippe Clément M. Joël Pauchet M. Arnaud Morin Mme Béatrice Icard
Other concerned Departments, Services, Laboratories	M. Othman Ladhari Mme Marion Chandris M. Pascal Schott

RULES FOR DOCUMENT MANAGEMENT AND CONFIDENTIALITY::

Based on the privacy statement shown at the bottom of the page, this document must be managed according to the guidelines described below, in accordance with contractual requirements.

FREE DISTRIBUTION:
This document may be distributed to other third parties than those defined in the distribution list.
It must be distributed unchanged and in its entirety and include the issuer's attribution and credit. This corresponds to the type of licence 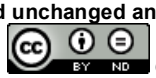 **defined by** http://creativecommons.org/licenses/.
However, recipients are requested to exercise sound judgement when redistributing the document.

CONFIDENTIAL:

This document may not be reproduced or transmitted to third parties without the express authorization of the issuing contractor.
The decision to remove the CONFIDENTIAL nature of the document rests with the issuer or comes into effect after the period specified in the contract.

CONFIDENTIAL "PROJECT NAME":

This document may only be distributed, within staff of recipient contractor, to individuals in the project team and to individuals who require access in the course of their duties (need to know basis). Contractors are required to implement the necessary measures for complying with these distribution rules, which may be based on restricted distribution measures.
This document may not be reproduced or transmitted to third parties without the express authorization of issuing contractor.
The decision to remove the CONFIDENTIAL "PROJECT NAME" nature of the document rests with the issuer or comes into effect after the period specified in the contract.

RESTRICTED DISTRIBUTION:
This document may only be distributed to individuals in the project team and individuals who require access in the course of their duties (need to know basis).
This document may not be reproduced or transmitted to third parties without the express authorization of the issuing contractor (i.e, the appendix of security, necessarily signed for a project with restricted distribution).
The management of information must comply with the requirements in Appendix 3 of Interdepartmental General Instruction IGI 1300 (http://www.ssi.gouv.fr)**, including:**

- Individuals must be informed about the rules of confidentiality.
- The information and drafts used in drawing up the document must be labelled with the words "RESTRICTED DISTRIBUTION" and managed as such (in particular, with a recording specifying the character RD of the document).
- The document and information used in drawing up the document must be kept under lock and key. In particular, the documents, when not in use, must be filed in a locked cabinet.
- The document may be sent externally by letter in a double envelope (it is advisable to use a cloth lined or confidential envelope). The inner envelope must bear the words RESTRICTED DISTRIBUTION, the name of the recipient and the document reference. The outer envelope must include only the information required for the letter to be sent (the department sending the letter and the address of the recipient). It must be sent with acknowledgment of receipt. This sending should be accompanied with a dispatch note identifying the addressees.
- The IT systems for processing, storing or transmitting the information are subject to security accreditation. When the networks or systems used are not able to guarantee confidentiality, the information is encrypted by methods approved by ANSSI (French Network and Information Security Agency). This results in the encryption of emails, computer directories, USB keys, servers, etc. using encryption approved by ANSSI. The list of equipment approved by ANSSI may be consulted on their web-site at http://www.ssi.gouv.fr
- It is the responsibility of the holder to destroy the document by shredding or incineration.
- The decision to remove the words RESTRICTED DISTRIBUTION rests with the issuer or comes into effect after the period specified in the contract.

ABSTRACT

In the face of growing environmental concerns and the need to mitigate climate change, the search for sustainable energy sources has reached a critical juncture. One of the most promising options that has garnered considerable attention in recent years is hydrogen. However, the debate on whether hydrogen can truly be considered "green" due to its production methods persists. Nonetheless, the importance of developing systems to harness chemical energy from hydrogen is undeniable, and fuel cells offer a viable solution for electrochemical energy conversion. If generated using renewable energy, such as solar or wind power, it becomes "green hydrogen," offering a clean and sustainable energy option.

The demand for mobility in modern society necessitates a shift towards sustainable transportation solutions. Traditional internal combustion engines reliant on hydrocarbons contribute significantly to air pollution and global warming. Electrochemical power conversion using fuel cells presents a compelling alternative. By combining hydrogen with oxygen from the air, fuel cells produce electricity, heat, and water, emitting only clean water vapor as a byproduct. This emission-free characteristic makes fuel cells an ideal solution for sustainable mobility.

Among various fuel cell types, Proton Exchange Membrane Fuel Cells (PEMFCs) stand out as a promising technology. They operate at relatively low temperatures, typically around room temperature, which offers advantages such as rapid start-up and high conversion efficiencies. While PEMFCs have shown immense potential, they do face certain challenges, particularly transport limitations within the cell. Transport restrictions can adversely impact cell performance and efficiency, which is why addressing these issues is crucial to optimize PEMFC operations.

In the context of this ongoing research project, the objective is to measure and model the transport limitations inside PEMFCs. By gaining a deeper understanding of these limitations, researchers can devise strategies to minimize their impact and enhance the overall performance of the fuel cells. Successful optimization of PEMFC operations will contribute to the wider adoption of fuel cells in sustainable mobility applications.

Table of contents

LIST OF FIGURES

LIST OF TABLES

1. INTRODUCTION

1.1 CEA

The French Alternative Energies and Atomic Energy Commission or CEA (French: Commissariat à l'énergie atomique et aux énergies alternatives), is a French public government-funded research organization in the fields of energy, defense and security, information technologies and health technologies.

It was founded in 1945, to strengthen French defense against the new nuclear powers like America. The decision to establish the organization was taken shortly after the bombings in the cities of Nagasaki and Hiroshima in August 1945. In September 1945, the decision was taken to establish a research organization dedicated just for atomic energy in France. So CEA was set up in October 18, 1945 by General Charles de Gaulle and headed by Jean Frédéric Joliot-Curie[1].

In December 2009, French President Nicolas Sarkozy changed the name of CEA from Commissariat à l'énergie atomique (Commission for Atomic Energy) to Commissariat à l'énergie atomique et aux énergies alternatives (English: Commission for Atomic Energy and Alternative Energies) reflecting change in main purposes of the establishment. This change was effective from March 2010 [2].

CEA plays an active and important role in the innovation and research in basically four main areas:

- Low carbon energies
- Technologies for information and health
- Large research infrastructures
- Defense and global security

1.1.1 CEA Grenoble

It was founded in 1956 by the initiative of Louis Néel , Nobel Prize in Physics , and owned three atomic batteries until the end of the 1990s. In the year 2000, the first atomic pile was stopped and CEA Grenoble began in the new direction under the new leadership of director Jean Therme. The activities were redirected towards the nanotechnologies, alternative energies, and health.

In 2013 it became the headquarter of CEA Tech. This center of CEA offers a very rich scientific, industrial and research environment. It devotes most of its research to development of innovative solutions in the fields of energy, health, information and communication. It was ranked as the "Top 25 Global Innovators in public arena in the world"[3].

CEA Grenoble contributes to the 70% of the patent applications of the entire CEA. In 2018 the Grenoble site of CEA inaugurated the first French unit for the industrial production of renewable hydrogen as the part of the project HyWay.

1.1.2 LITEN

The Innovation Laboratory for New Energy Technologies and Nanomaterials (LITEN) is a CEA specialized research institute dedicated to the new alternative energy technologies. It is one of the largest European research centers dedicated in the field of the energy transition.

One of the missions of the institute is to design production, storage, transport and conversion technologies for the deployment of the hydrogen sector.

CEA-Liten has various agreements with companies and institutions that are linked to energy sector. It is also involved behind the creation of about 10 start-ups in various field of energy since 2010. It has the Carnot label that is awarded to the public research laboratories carrying out outstanding research in public-private partnerships.

1.2 Fuel Cells

Fuel cells are a highly efficient and sustainable technology for energy conversion, and hydrogen is an excellent clean energy carrier. So, Proton Exchange Membrane Electrode Fuel Cell (PEMFC) has a great potential in the greenhouse gas emission reduction and transitioning to sustainable energy and decreasing the dependence on the hydrocarbons as the main source of energy [4].
Fuel cells and Hydrogen are going to become major contributors to a competitive economic growth in the coming time mainly in Europe as well for energy stationary applications as for transportation. The ongoing crisis of the availability of natural gas due to socio-political crisis, and the increasing rates of emissions are driving the transition process.
The major companies when it comes to sustainable mobility including Toyota, Honda, Hyundai are pushing for the advanced and economic models, with comparable cost to the Battery Electric Vehicles (BEVs). The most popular models powered by PEMFC include the Toyota Mirai, Honda Clarity, and Hyundai Nexo. The advantages of the fuel cell vehicles include the longer driving range with a shorter refuelling time which is only a few minutes, giving more autonomy to the user. When compared to Lithium batteries, the chemistry is simpler and the solid electrolyte makes the disassembling easier, faster and safer. The recycling and repurposing is also easier compared to the batteries. Considering the all the advantages that PEMFC has, it's the preferred technology for the mobility applications especially for the heavy-duty applications. A large deployment could be predicted by 2025-2030[5]. The main advantages of PEMFC technology are [6]:

- High energy conversion efficiency 50-60%
- High power density of the stack: ~4kW/kg
- High energy density: 500-600 Wh/kg for the system
- Flexible: operating temperature between -20 and 90°C
- Fast refueling time

The main limitation to the use is that the performance and durability of the PEMFC system can't be predictive because of the complexity and non-linearity of the system. This is an area of research, with the major obstacle that the PEMFC system is non-linear multiphysics system, so it is difficult to understand the interactions at the microscopic and macroscopic levels. The goal of this study is to better understand the limitations inside the PEMFC system.
The extensive demand that is predicted for this application calls for the existing technology to be much cheaper with better performance, lifespan. It is important to improve the power density, while simultaneously decreasing the cost of the components, especially working to decrease the Platinum loading with better performances. As Pt is a critical raw material, so it is desirable to have high power densities, high current densities, higher durability at low Pt loadings [6]. Also, searching for new catalyst material is an open possibility for making the system more economic and durable with good performance [4].

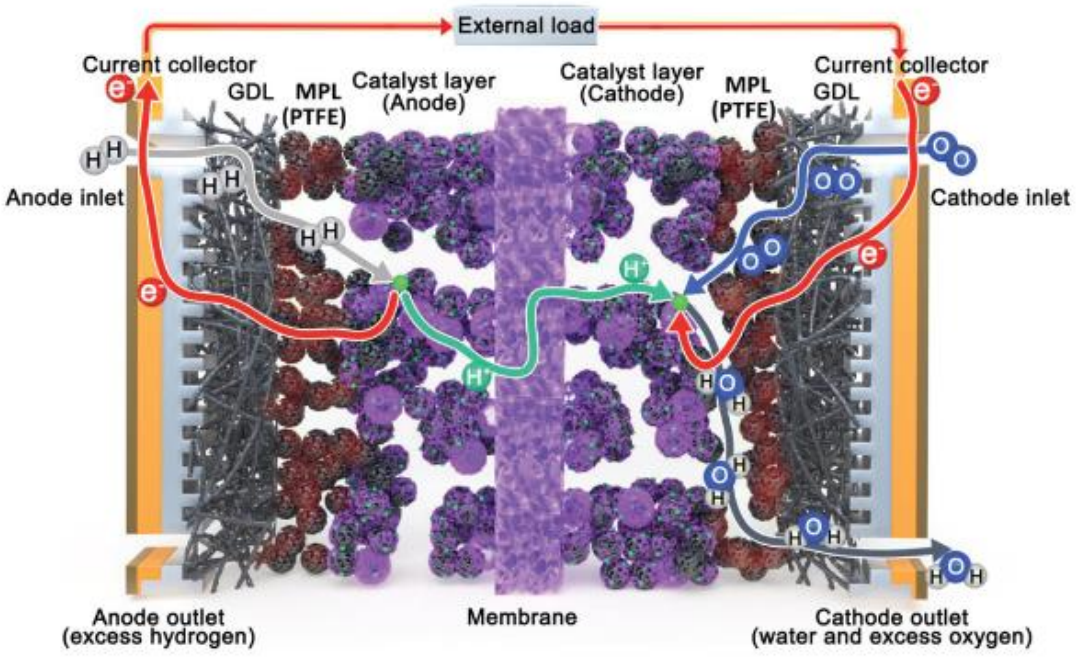

Figure 1: Schematic of an acid PEFC showing the different layers, their compositions, and reactant transport pathways [6]

The basic chemistry of PEMFC is simple with the input of Hydrogen at the anode and the Oxygen at the cathode. This leads to the reaction between the hydrogen ion and oxygen at the cathode leading to the conversion of chemical energy liberated during the electrochemical reaction into electrical energy. The simplified electrochemical reactions occurring at each electrode can be stated as below:

$$H_2 \xrightarrow{anode} 2H^+$$

$$2H^+ + O_2 \xrightarrow{cathode} H_2O$$

The cross section of the single PEMFC cell with different domains is shown in the Figure 1. The different domains that have different functions which are discussed in the next section. For the different cell components various types of models should be found depending on the applied physics and the geometry.

1. Membranes (MB):
   The main function of the membrane to transport protons from the anode to cathode.
   For the membranes are generally made of perfluorinated polymer materials. The models deal with sorption i.e., the water concentration inside the membrane, generally quantified by the relative humidity which affects the transport properties of the membrane.

2. Gas Diffusion Layer/ Microporous Layer (GDL/MPL)
   The main function of GDL is to transport the gas, electrons, heat and water in the fuel cell. It has two parts, the macro-porous substrate and the micro-porous layer. The approaches

towards considering the physics in this domain may be based on one of the following approaches:

a. Continuous Media: This considers averaged physical properties of GDL and MPL, which may lead to inaccuracies.
b. Lattice Boltzmann Model: This considers the complex porous structure of GDL and MPL to simulate the flow in the media. This considers the real morphology of the materials.
c. Pore Network Model: This model uses the physio-chemical properties such as porosity and pore size distribution to describe the transport phenomena.

3. Catalyst layer (CL)

The main function of the catalyst layer is to enhance the rate of reaction both at anode and cathode. The oxygen reduction reaction at the cathode is the limiting reaction because of the slow kinetics [7]. The catalyst used in our case is Platinum, and the Pt loading at the cathode is about 2-3 times more than the anode. This is the most interesting domain for us, as it controls the electrochemistry and mass transport properties:

a. Mass transport: Some models discretize the catalyst layer and the Pt particles supported on carbon. Other models consider an agglomerate scale approach with the consideration that the catalyst layer is made of spherical or cylindrical Pt-C embedded in the ionomer film.
b. Electrochemistry: The focus is on the triple phase boundary interface on the surface of the Cathode Catalyst Layer (CCL). There ae two, 2-phase boundaries in reality, the interface between Platinum in solid phase, hydrogen ion and dissolved oxygen gas in the electrolyte phase and the oxygen gas and electrolyte interface as shown in the figure 2. As the Oxygen Reduction Reaction (ORR) is limiting, the understanding of the mechanism of reaction on cathode is important for the quantification of these limitations.

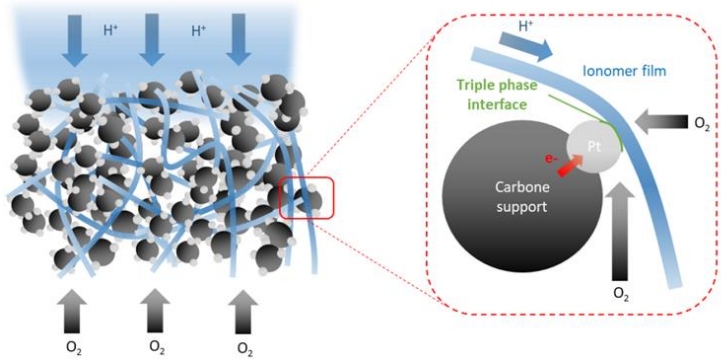

Figure 2: Cathode Catalyst layer with the three-phase interface description

Nernst and Butler-Volmer approaches in a single step reaction ae often used to describe Hydrogen Oxidation Reaction (HOR) and Oxygen Reduction Reaction (ORR) [8]. The reaction chemistry of ORR is much more complex involving formation of several intermediate species [9].

The Nernst and Butler Volmer does not consider the surface state, coverage and dynamic evolution. Thus, a more evolved approach considering the multiple steps of the reaction and partial surface coverage with the adsorption and desorption of the reacting species on the electrocatalytic sites must be considered. This description is also useful when describing the mechanisms like aging and degradation of the catalyst, impurities on the active surface that might affect the performance of the catalyst.

4. Biploar Plates (BP)
   The main function of the Bipolar plates is to uniformly distribute fuel gas and air, conduct current from cell to cell, remove heat from the active area, and prevent leakage of the gases and coolant. The focus of this study is not much on the bipolar plate.

It is clearly noticed that the research and development must focus more on the Membrane Electrode Assembly (MEA), although there is research going on other components as well. As, MEA is the heart of the fuel cell and the center of the electrochemical conversion and it is responsible for about 60% cost for the entire stack.

As we know the electrochemical reaction at the cathode is limiting, so the impacts of the Cathode Catalyst Layer on the entire cost is prominent, as the Pt loading on the cathode is about three times higher than the anode. The Cathode Catalyst Layer (CCL), with the Oxygen Reduction Reaction (ORR) takes place on the active Pt sites, can represent up to 35% of the total cost of the stack [10]. In addition, the CCL affects the performance of the stack, contributing to about 70% of the total losses in the stack [11] as shown in figure 3 and 4. The losses are from the slow kinetics of the ORR, transport limitations that limit the full utilization of the active Pt area available. There are also degradation and parasitic reactions, corrosion that are responsible for lower performances [12].

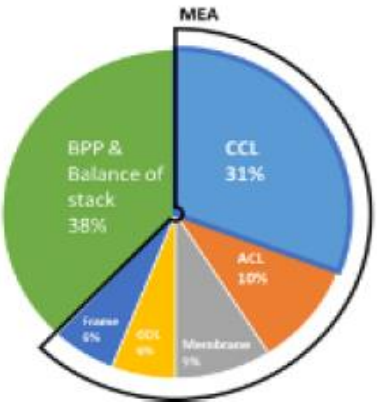

Figure 3: Effect of CCL on the cost of stack[10]

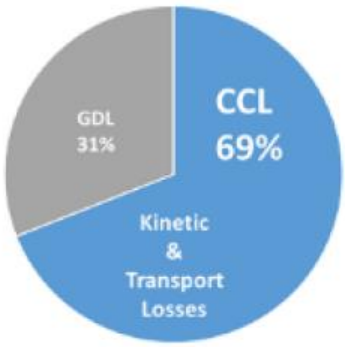

Figure 4: Effect of CCL on the performance of MEA [11]

There are complex processes that are coupled in the CCL making it a major limiting component in the performance of PEMFC.

Many studies and research work are mainly dedicated on improving these limitations. The design and optimization of the performance currently rely on the tuning of the structural and operating parameters on the trial-and-error methods. These methods are based in the empirical criteria and there is much less knowhow on the technical approaches that can be done only with the deeper

and holistic understanding the system [13]. There aren't any models that are available for predicting the performance and durability of the PEMFC that are fully validated and reliable. The modelling of the performance a lifetime of PEMFC is one of the hottest areas of research in the field of electrochemical systems and sustainable mobility. Modelling of the performance entails clear understanding of the limitations inside the system.
Modelling the mass and heat transport limitations in PEMFCs is a complex task as the PEMFCs are non-linear, complex systems with multi-physics phenomenon at different domains of the geometry at different rates. These phenomena are lumped together and the independent analysis is difficult. There are internal core components and external operating conditions that affect the performance.

1.3 FURTHER

The biggest challenge in designing an efficient PEMFC stack is having a better understanding of the relevant physical and electrochemical phenomena.
The FURTHER-FC project aims at developing better understanding of the transport limitations in the PEMFC. The focus is on the CCL as the mainly limiting factor in the performance. The aim is to improve the cost, durability at low Pt loadings.
The end result desired is to bring the cutting-edge technology at the experimental and the modelling level together with the fundamental characterization coupled with the advance models on the CCL, in order to understand the transport limitations and electrochemical issues at various scales of the CCL. This a combined research initiative with the collaboration with various international research institutes and organizations.
This thesis is based on the experimental work, improvements in the electrochemical models, which include the domain, geometry simulated and different physics modelled within the domains. In this project work is mainly in the area of the transport limitations of protons and oxygen transport.
PEMFC electrode development has drawn many researches as it is a crucial material driving, the electricity production of the whole system, and its durability. Most electrochemical limitations come from cathodic electrode since the Oxygen Reduction Reaction (ORR) and Oxygen transport are slow compare to Hydrogen Oxidation Reaction (HOR) and Hydrogen transport [14].
One of the strengths of the mathematical models is to quantify the contribution of each mechanism by choosing relevant operating conditions and scales, which is a difficult to achieve experimentally. The most challenging step in the modelling of the system is to identify the underlying complex physics in each domain and to capture the complex interaction of different phenomenon in PEMFC operation. Different studies have been conducted to study particular mechanisms for instance ORR mechanisms or particular domains like catalyst layer operation[15].

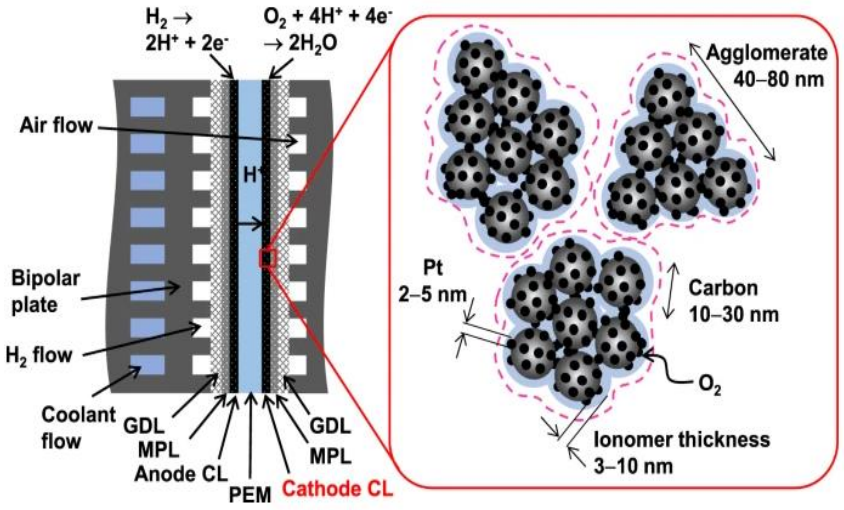

Figure 5: The Schematic showing the Cathode Catalyst Layer [14]

2. METHODOLOGY

This study is a part of FURTHER_FC, as discussed above. I worked on the measurement and modelling of the proton and oxygen transport limitations. The approach is both experimental and simulation based. The idea is to take the experimental data and simulate the curves of Polarization and Electrochemical impedance Spectroscopy curves. The fitting of the polarization curve at low current density (<20 mA/cm^2) gives the values of the parameters responsible for the kinetics of ORR. The sensitivity study of the EIS curves by varying several parameters helps us understand the key parameters that control the shape of EIS curves. The Limiting current analysis is a good method for measuring the oxygen transport resistance. The effect if various operation and characteristic parameters were also seen in this study.

Mathematical modeling is a relevant choice of technology in understanding the system and saves a lot of time and cost of development.

Specific and accurate physical modeling often leads to simulation with restricted domain model, which motivates the development of numerous macro-scale models for the cell level, including all of the components and relevant process. Several models have been developed and studied that cover all of the relevant scales from the atomic scale up to the system level [16].

2.1 Experimental set up

2.1.1 Differential fuel cell

For the purposes of the current study, we assume that we maintain uniform concentration of the constituent gases in the flow channels. This is the condition of operation of differential cell. No cell in reality is perfectly differential, but this condition can be approached in small active surface area and high reactant stoichiometries (*26 times at 3A/ cm^2)*. High stoichiometric conditions are required to make sure that consumption of reactant in almost uniform in the down channels, and

the small areas ensure that high pressure gradients aren't created because of the high flow rates, so there is not much variation in the relative humidity across the cell. The rib- channel widths are small to avoid any heterogeneities in the system and a homogeneous operation is maintained in the perpendicular direction. The operations are carried out at 80C, we are varying the total pressure at the cathode and anode, and the partial pressure of oxygen at the cathode inlet. The Relative humidity humidity is aloso changed to study the effects.

2.1.2 MEA Composition

The table 1 shows the composition of MEA. The materials were selected for the state-of the-art automotive applications. As GDL, we selected the Sigracet 22BB from SGL (Germany). It is specifically designed for the Automotive application with a thickness of 215 µm. The GDL is already prepared with PTFE (5%) and with a MPL layer on one side.

Tableau 1: Material and Composition of Reference MEA

	Cathode	Anode
GDL	Sigracet 22BB (SGL)	
Membrane	NC700 (Chemours)	
Catalyst	TEC10E50E 46.2% Pt on High surface area carbon (Tanaka)	
Ionomer	D2020CS / 20% Nafion dispersion (Chemours)	
I/C weight ratio	0.8	
Loading	0.2 mg_{Pt}/cm^2	0.1 mg_{Pt}/cm^2

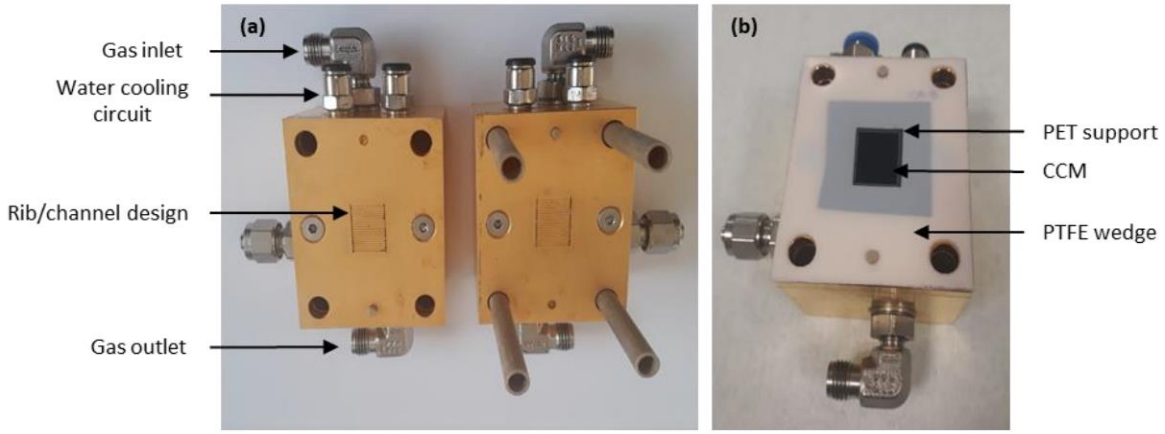

Figure 6: (a) Differential Cell Assembly (b) MEA assembly

Membrane and ionomer are supplied by Chemours (Project partner). We selected the NC700 as the membrane whose thickness is 15 µm with a reinforcement layer. D2020CS (20% Nafion® dispersion) is selected as ionomer for the cathode and anode catalyst layer.

The reference catalyst is supplied by Tanaka Kikinzoku. We selected the TEC10E50E (46.2 wt% Pt on high surface area carbon) which is a state-of-the-art material in the PEMFC community. Based on state-of-the-art and internal knowledge in TME, the ionomer/carbon (I/C) weight ratio is set to 0.8. Regarding catalyst loading, cathode amount is set to 0.2 mg_{Pt}/cm^2 and anode is set to 0.1 mg_{Pt}/cm^2.

2.1.3 Fabrication Process

The MEAs are assembled by TME and supplied to the different partners for characterization and evaluation. Here we describe the method for preparation of the ink, coating and final assembly.

a) **Ink preparation**: Catalyst, solvent and ionomer is weighed using a precision microbalance. Amount of solvent and water is calculated in order to have a 10% solid content and a solvent to water ratio of 1.3. We use Diacetone Alcohol as added solvent. Components are introduced in a container and mixed by using a centrifugal mixer (Thinky) at 2000 RPM for 5 min in order to obtain a homogeneous mixture (Premix).
In order to decrease particle size distribution and increase the dispersion of the ink, the Premix is further homogenized by using ball milling. The ink is introduced in a zirconia jar together with zirconia beads (1 mm) in a mass ratio of 0.25. Ink is processed at 400 RPM for 4 hours.
As final step, the ink is introduced in a container and mix under vacuum (Thinky) at 2000 RPM for 5 minutes in order to degas the ink.

b) **Coating**: Catalyst layer is prepared by spreading the ink using a knife coater on a PTFE substrate. More precisely, the PTFE sheet (30 x 30 cm) is fixed on a glass plate by using solvent capillarity. PTFE sheet is brushed in order to render it flat. For cathode coating with a loading of 0.2 mg_{Pt}/cm^2 the knife gap is set to 80 µm. For anode coating with a loading of 0.1 mg_{Pt}/cm^2 the knife gap is set to 40 µm. 2-3 ml of ink is spread in front of the knife. The knife is moved on the substrate at a speed of 12.5 mm/min. The total coated area is around 200 cm^2. The coating is dried in oven at 80°C for 1h.

c) **Assembly**: Cathode and anode coatings dimensions are 90 mm x 90 mm. Membrane is cut slightly larger than catalyst layer (100 x 100 mm). Cathode, membrane and anode is assembled and centered in this respective order. Catalyst layers are transferred from PTFE to Membrane by hot press (140°C, 10 bar, 3 min).
The 3-layer MEA is supplied to the partner together with the GDL. MEA and GDL by each partner to specific size depending on cell configuration.

2.2 Modelling

The model that is used in this thesis has been developed under the project called EUROPIUM, which stands for the ElectRochemistry OPtimization Understanding Modelling. This is a numerical simulation platform that is used to simulate the performance of the fuel cell using COMSOL Multiphysics software for the commercial code and MATLAB software to build the models.

- The 2D rib-channel model used from the platform considers gas flows from the inlet to outlet and discretized as the separate domains of GDL, MPL, CL and MB, through the thickness of MEA.

- A 1D rib channel model is the simplified 2D model through the thickness version, by the application of the simple boundary conditions at the channel. This is discussed in the section later.
- A pseudo 3D description of the whole cell is superimposing 2D layers [17].

In the report we will discuss the 2D rib channel and then it can be simplified to get 1D or improved to get 3D model as per bargain between the simulating time and accuracy needed.

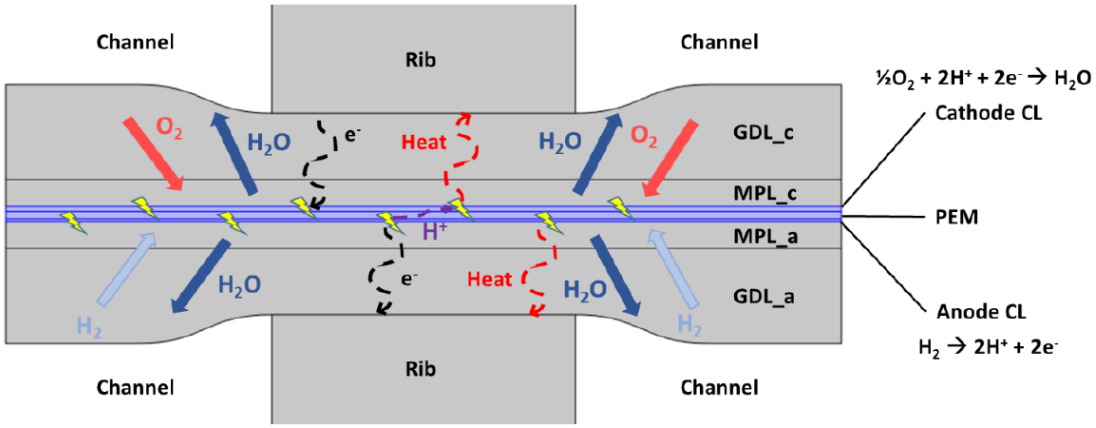

Figure 7: The 2D cross-section of MEA showing the rib-channel

The 1 D model is just the simplification of the 2D model, and we do not apply the Navier-stokes in the channels and just some simple boundary conditions. The geometry and explanation of the 1D model:

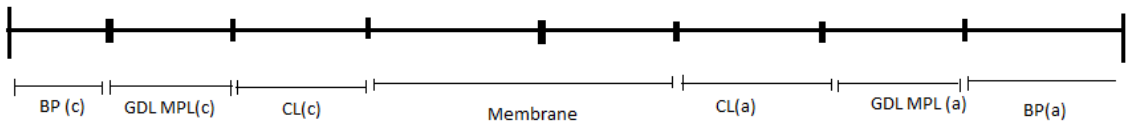

Figure 8: Different domains in MEA assembly for the 1D PEMFC model

The symmetry line is through the center of the membrane layer and the right side of the symmetry line is considered positive for the consideration of the length measurements and left is negative.
The thickness of the membrane on the right $ep_{MB}/\,2$ and to the left $-ep_{MB}/\,2$.
The thickness till the boundary of Catalyst Layer on the right $ep_{MB}/\,2 + \mathrm{ep}_{\mathrm{CL_c}}$ and to the left $-ep_{MB}/\,2 - \mathrm{ep}_{\mathrm{CL_a}}$
The thickness till the boundary of the Gas Diffusion Layer on the right $ep_{MB}/\,2 + \mathrm{ep}_{\mathrm{CL_c}} + ep_{MPL} + ep_{GDL}$ and to the left $-ep_{MB}/2 - \mathrm{ep}_{\mathrm{CL_a}} - ep_{MPL_a} - ep_{CL_a}$

The thickness till the boundary of the Bipolar Plate on the right $ep_{MB}/2 + \mathrm{ep}_{\mathrm{CL_c}} + ep_{MPL} + ep_{GDL} + ep_{BP_c}$ and to the left $-ep_{MB}/2 - \mathrm{ep}_{\mathrm{CL_a}} - ep_{MPL_a} - ep_{CL_a} - ep_{BP_a}$
The general equations governing the mass transfer has been simplified for the 1D model. Different regions would have different phenomenon physical and chemical. The results is a complex interaction. For the 2 D model we consider the following interactions

Tableau 2: Different physical interactions in different domains in 2D

Physics	Chanel (CH)	Gas Diffusion Layer (GDL)	Microporous Layer (MPL)	Catalyst Layer (CL)	Membrane (MB)	Bipolar Plate (BP)
Navier-stokes	✓					
Diffusion	✓	✓	✓	✓	✓	
Ionic Transport				✓	✓	
Electric Transport		✓	✓	✓		✓
Electrochemistry				✓		
Thermal		✓	✓	✓	✓	

So the modelling has to be performed for each domain

2.2.1 Channels

The composition in the cathode side is a mixture of O_2, N_2 *and* H_2O (g) and for the anode side is a mixture of H_2, N_2 *and* H_2O (g). In the channels, convection phenomena occurs and phase is gaseous. The NS equations of written for the Newtonian fluid assumed in the channels. The relation between the mass average velocity $\vec{u}$ and volume average velocity $\vec{U}$ as given by Brenner [10]

$$\vec{U} = \vec{u} - \frac{\sum M_i \overrightarrow{N_i^d}}{\rho_g} \quad (1)$$

Where ρ_g is the density of the gas phase, M_i is the Molar Mass of different components, $\overrightarrow{N_i^d}$ is the diffusive flux of the different components.
So, the Naiver Stokes for the channel can be written as

$$\rho_g\left(\frac{\partial \vec{u}}{\partial t} + (\vec{u}\,.\nabla)\vec{u} + M_v S_{cond}\vec{u}\right) = -\nabla\vec{p} + \nabla.\left(\mu_g\left(\nabla\vec{U} + \left(\vec{U}\right)^T\right) - \frac{2}{3}\mu_g(\nabla.\vec{U})I\right) \quad (2)$$

S_{cond} is the condensation term for the water vapor, p is the relative pressure, μ_g is the dynamic viscosity, I is the identity matrix. The molar balance for the gas phase

$$\frac{\partial c_g}{\partial t} + \nabla.\left(c_g\vec{U}\right) = \sum_i S_i \quad (3)$$

where $S_i = S_{cond}$ for the water vapor, and
$S_i = 0$ for the other gaseous components.
c_g is the total concentration of gases.
Now the mass balance for each gas component in equilibrium with the continuous porous media, so the relation between the volume average velocity and the total molar flux of the component can be written as

$$\vec{U} = \frac{\sum_i \overrightarrow{N_i^{GDL}}}{c_g} \quad 4$$

Where c_g is the total concentration of gases, and
$\overrightarrow{N_i^{GDL}}$ is the total molar flux of the component i.
Now the component mass balance could be written as a simple equation

$$\frac{\partial c_g}{\partial t} + \nabla.\left(\overrightarrow{N_i^d} + c_g\vec{U}\right) = S_i \quad 5$$

At the channel and GDL interface, writing the continuity for the flux of each component

$$\overrightarrow{N_i^d} + c_g\vec{U} = \overrightarrow{N_i^{GDL}} \quad 6$$

The molar flux of the component $\overrightarrow{N_i^d}$ can be calculated from the solution of the Stefan-Maxwell's equation

$$c_g\vec{\nabla}X_i = \sum_i \frac{X_i\overrightarrow{N_j^d} - X_j\overrightarrow{N_i^d}}{D_{i,j}} \quad 7$$

Given that, from the definition of diffusion

$$\sum_i \overrightarrow{N_i^d} = 0 \quad 8$$

Where, $D_{i,j}$ is the binary diffusion coefficient.

The boundary conditions
At the inlet of channel:
The gas volume velocity is imposed, where $\vec{U}$ and $\vec{V}$ are the x and y components of the velocity vector.

$$-\vec{U} + \frac{\vec{u}c_{g,0}}{c_g} = 0 \quad (9)$$

$$-\vec{V} = 0 \quad (10)$$

At the outlet of channel:
The pressure is imposed,

$$\rho_g\left(\frac{\partial \vec{u}}{\partial t} + (\vec{u}\,.\nabla)\vec{u} + M_v S_{cond}\vec{u}\right) = -\nabla\vec{p} + \nabla.\left(\mu_g\left(\nabla\vec{U} + \left(\vec{U}\right)^T\right) - \frac{2}{3}\mu_g(\nabla.\vec{U})I\right) \quad (11)$$

$$0 = -\vec{p} + \left(\mu_g\left(\frac{\partial \vec{U}}{\partial x} + \frac{\partial \vec{U}}{\partial y}\right) - \frac{2}{3}\mu_g\left(\frac{\partial \vec{U}}{\partial x}\right)\right) \quad (12)$$

$$-p = 0 \quad (13)$$

Walls:
Velocity is zero at the walls of the channel

$$-\vec{U} = 0 \quad (14)$$

$$-\vec{V} = 0 \quad (15)$$

Mass average velocity is constant at the MEA/channel interface

$$-\vec{u} + \vec{u}_g^{GDL} = 0 \quad (16)$$

$$-\vec{v} + \vec{v}_g^{GDL} = 0 \quad (17)$$

2.2.2 Electrochemistry

The effects of the local responses of oxygen reduction reaction at the cathode and hydrogen oxygen reduction at the anode
Foe the half reactions on the electrodes

$$\sum_j v_j . M_j^{z_j} \underset{ox/red}{\Longleftrightarrow} n.e^- \quad (18)$$

Where, z_j is the charge of the specie M_j and $v_j$is the stoichiometry coefficient of the specie M_j
The current density produced can be estimated by the Butler-Volmer's equation[8]

$$j_r = j_o\, a_v \left[\exp\left(\frac{\alpha n F}{RT}\eta\right) - \exp\left(\frac{-(1-\alpha)nF}{RT}\eta\right)\right] \quad 19$$

Where, η is the overpotential, α and $1-\alpha$ are the symmetry factor of the reaction and j_o is the exchange current density. j_o is dependent on the local specie activities and reaction kinetics.

$$j_o = nF(k_{ox}^o)^{1-\alpha}(k_{red}^o)^{\alpha}.\left(\prod_{v_j>0}\left(a_j^{v_j}\right)\right)^{1-\alpha}\left(\prod_{v_j<0}\left(a_j^{-v_j}\right)\right)^{\alpha} \quad 18$$

Where, $a_j$is the activity of the specie, $k_{ox/red}^o$ are the reaction rate coefficients, depending on the Gibbs free energy

$$k_{ox}^o = k^0 \exp\left(\frac{\Delta G_{ox}}{RT}\right) \quad 21$$

$$k_{red}^o = k^0 \exp\left(\frac{\Delta G_{red}}{RT}\right) \quad 22$$

Where the constant k^0 is given by

$$k^0 = \frac{\mathrm{k_b} T}{s_0 N_A h} \quad 23$$

Where, $\mathrm{k_b}$ is the Boltzmann constant, h is the Plank's constant, s_0 is the average Pt surface per reaction site, N_A is the Avogadro number.

$$\Delta G_{ox} = \Delta H_{ox} - T\Delta S_{ox} \quad 19$$

$$\Delta G_{red} = \Delta G_{ox} + \Delta G \quad 25$$

The ΔG can be estimated from the Lampinen and Formino [18]
The overpotential η is defined as

$$\eta = (\Psi - \Phi) - \left(\Psi_{\mathrm{eq}} - \Phi_{eq}\right) \quad 26$$

where, Ψ is the electrode potential and, Φ is the ionic potential

$$\left(\Psi_{\mathrm{eq}} - \Phi_{eq}\right) = E \quad 27$$

$$\eta = (\Psi - \Phi) - (E) \quad 28$$

E is the standard electrode potential, depending on the temperature, pressure and concentrations following the Nernst's Equation:

$$E = -\frac{\Delta G^0}{nF} + \frac{RT}{nF}\log\left(\prod_{v_j} a_j^{v_j}\right) \quad 29$$

Where,

$$\Delta G^0 = \Delta H^0 - T\Delta S^0 \quad (30)$$

We assume that there is equilibrium between the gases in the electrolyte and porous interface.

$$C_i^{eq} = P_i H_i \quad (31)$$

Where H_i is the Henry constant and P_i is the partial pressure [19]. The dissolved specie i activity can be expressed in terms of H_i as

$$a_i = \frac{H_i c_i}{P^o} \quad (32)$$

$$a_{H_2O} = \frac{P_{vap}}{P_{sat}(T)} \quad (33)$$

P^o is the standard pressure.

$$P_{vap} = c_{vap} RT \quad (34)$$

The permeation currents at the anode and cathode
$J_{p_a} = 0$, for the anode side catalyst layer
$J_{p_c} = \frac{\overrightarrow{N_{H_2}^a}.2.F}{t_{CL_c}}.\vec{n}$, for the cathode side catalyst layer
t_{CL_c}, is the thickness of the cathodic catalyst layer

2.2.3 Porous media

The diffusion component:
For the porous media, the effects of Knudsen and Darcy diffusion must be considered for good accuracy. So we use the Young and Todd approach[20], the equations are similar with the Stefan Maxwell equations with the additional inclusion of ε which is the porosity and τ the tortuosity.

$$\frac{c_g \varepsilon \vec{\nabla} X_i}{\tau^2} = \sum_i \left[\frac{X_i \overrightarrow{N_j^d}}{D_{A_{ji}}} - \frac{X_j \overrightarrow{N_i^d}}{D_{A_{ji}}} \right] \quad (35)$$

Mathematically it's the interpolation between the pure gaseous diffusion and Knudsen diffusion

$$\frac{1}{D_{A_{ij}}} = \frac{1}{D_{ij}} + \frac{1}{D_i^k} \quad (20)$$

Where the estimation of Knudsen diffusion coefficient could be done using the relation

$$D_i^k = \frac{2}{3} R_p . \sqrt{\frac{8RT}{\pi M_i}} \quad 37$$

Where, R_p is the pore radius.

The convection component:

The overall pressure drop in the gas phase can be expressed in terms of the overall convection coefficient A_A

$$\frac{\varepsilon}{\tau^2} \vec{\nabla} P_g = -A_A \sum_i \sqrt{\vec{M_i}} \vec{N_i} \quad 38$$

A_A is the overall convection coefficient in the porous media which is the effect of pure convection term depending on the permeability k and Knudsen diffusion term related with the pore radius R_p

$$\frac{1}{A_A} = \frac{1}{A_C} + \frac{1}{A_K} \quad 39$$

Compared to the original relation [20], the value of A_c has been modified,

$$A_c = \frac{\mu}{c_g k \sum_i x_i \sqrt{M_i}} \quad 40$$

$$A_k = \frac{3}{4 R_p} \sqrt{\frac{\pi RT}{2}} \quad 41$$

The mass balance for each species can be written as

$$\varepsilon \frac{\delta c_i}{\delta t} = \nabla . \vec{N_i} + S_i \quad 421$$

$S_i = S_{vap}^d + S_{cond}$, for the water vapor

$S_i = S_i^a$, for other gases

Where, S_{vap}^d, is the water adsorbed by the ionomer in the Catalyst layer and S_i^a is the dissolution rate for the gas in the ionomer of the catalyst layer.

At the interface between the Channel/GDL we can write the continuity of the concentration of the components can be written as

$$c_i^{CH} = c_i^{GDL} \quad 43$$

No net flux is assumed because of symmetry or insulation is considered at the interface of the channel and GDL.

$$\vec{N_i} . \vec{n} = 0 \quad 44$$

2.2.4 Electrolyte phase

Hydrogen diffusion is evaluated in the anode side catalyst layer and through the membrane. The crossover of hydrogen is considered while calculating the Open Circuit Voltage. Oxygen diffusion is only evaluated in the cathode catalyst layer, no effect oxygen is considered while calculating the crossover current [21].

The mass balance for each species can be written as

$$(1-\varepsilon)\varepsilon_{ionomer}\frac{\partial c_g}{\partial t} = -\nabla.\left(\overrightarrow{N_i^a}\right) + S_i^a + S_i \quad 45$$

$$\overrightarrow{N_{H_2O}^a} = \frac{n_d \vec{i_l}}{F} - D_w^a \vec{\nabla} C_{H_2O} \quad 46$$

Equation 46 is used or the water flux we have two components, electro-osmosis and diffusion, n_d is the electro-osmotic drag coefficient [22].

$\overrightarrow{N_i^a} = -D_i^a \vec{\nabla} C_i$, for other components only diffusion flux is applicable

$\overrightarrow{N_i^a}$ is modelled as source term on the right side of the equation because the agglomerated thickness e_{naf} is not discretized.

$S_i^a = \frac{D_i^a a_v}{e_{ionomer}}(C_i^{eq} - C_i)$, it is the source term that estimates the diffusion flux through the Nafion's film. This expression is applicable in Catalyst Layer.

$S_i^a = 0$, in the Membrane

Where, $a_v$is the specific surface area, S_i Is the source coming from the electrochemical reactions occurring at catalyst layer.

J_r, J_p are the Current density of the reaction and permeation respectively. So, the source terms for different species can be defined as follows

Tableau 3: The source terms for different chemical species

S_i (for different species)	Electrochemical source term	Domain of occurrence
S_{H_2}	$-\frac{J_r}{2F}$	Anode Catalyst Layer
S_{H_2O}	0	Anode Catalyst layer
S_{O_2}	$\frac{J_r + J_p}{4F}$	Cathode catalyst Layer
S_{H_2O}	$-\frac{J_r + J_p}{2F}$	Cathode catalyst Layer

The thickness of the ionomer can be calculated from specific surface area and Nafion content

$$e_{ionomer} = \frac{(1-\varepsilon)\varepsilon_{ionomer}}{a_v} \quad 47$$

The concentration of water inside the ionomer is defined as

$$C_{H_2O} = \Lambda . C_{SO_3^-} \quad 2248$$

The equilibrium concentration is estimated at the ionomer/pore interface is calculated by the relation [23]

$$\Lambda_{eq}(a_{H_2O}) = 0.043 + 17.81a_{H_2O} - 39.85a_{H_2O}^2 + 36a_{H_2O}^3 \quad 49$$

Where a_{H_2O} is the activity of water.

2.2.5 Electronic Transport

The charge conservation equation can be written domain of GDL, MPL, CL and BP.

$$\nabla.\vec{\imath_e} = -\nabla.(\sigma_e.\vec{\nabla}.\Psi) = S \quad 23$$

Where $\vec{\imath_e}$, is the electronic current, σ_e is the electronic conductivity, S is the source term. In the GDL and MPL there is no source term, in the catalyst layer on the other hand production and consumption comes from the reaction and permeation currents.
$S = 0$, in the GDL and MPL,
$S = J_r - J_p$, in the CL

2.2.6 Ionic Transport

The ionic transport term is evaluated only in the CL and the membrane.

$$\nabla.\vec{\imath_i} = -\nabla.(\sigma_i.\vec{\nabla}.\Phi) = S \quad 24$$

Where $\vec{\imath_i}$, is the ionic current, σ_i is the ionic conductivity, S is the source term. In the membrane there is no production or consumption of the ions, in the catalyst layer the direction of the ionic current is opposite of the electronic current.
$S = 0$, in the MB,
$S = -J_r + J_p$, in the CL
The calculation of the ionic conductivity in the membrane is given by the relation [24]

$$\sigma_i = \frac{(1-\varepsilon)\varepsilon_{ionomer}}{\tau^2}.\sigma_{i,m} \quad 25$$

Where $\sigma_{i,m}$ is the ionic conductivity of the nafion. We can see that ionic conductivity depends on the water content.
The total current is the sum of the electronic in the carbon phase and the ionic current in the nafion.

2.2.7 Thermal Balance

The terms that are considered are the conduction in the solid phase. The heat convection in the gas phase are neglected.

$$\rho c_p \frac{\partial T}{\partial x} + \nabla.\left(-\lambda \vec{\nabla} T\right) = \sum Q \quad (26)$$

Where c_p is the heat capacity, λ is the thermal conductivity and Q is the source term which is dependent on the domain under consideration.
At each electrode the heat of the reactions for the anode and cathode, can be related to the electric work and the heat as the following relation

$$\frac{\Delta H^0_{a/c}}{nF} J_r = W_e + Q_{reac} \quad (27)$$

Where $\Delta H^0_{a/c}$, is the enthalpy of hydrogen oxidation reaction at anode, or the enthalpy of oxygen reduction at the cathode, W_e is the electrical energy, and Q_{reac} and heat power generated from the reaction [21].
The local electrical energy produced in the CL is given by,

$$W_e = (\Phi - \Psi).J_r \quad (28)$$

The local heat produced from the reaction in the CL is given by,

$$Q_{rec} = \left((\Psi - \Phi) + \frac{\Delta H^0_{a/c}}{nF}\right).J_r \quad (29)$$

The heat produced by the permeation current on the cathode side

$$Q_{perm} = \frac{(-\Delta H^0_a + \Delta H^0_c)}{nF}.J_p \quad (30)$$

The joule heating term can be taken in each domain

$$Q_j = \frac{i^2}{\sigma_j} \quad (31)$$

Where i, is the local current in the domain, σ_j is the local electrical conductivity

3. ANALYSIS

This thesis work at CEA aims at measurement and quantification of the transport limitations of the oxygen and proton. The parameters related to the transport of protons in the catalyst layer are the tortuosity of the ionomer in the catalyst layer, and for the oxygen transport it is the tortuosity of the GDL, MPL, and CL. The goal is to see the effect of these parameters on the

transport limitations and find the values by fitting of Polarization and Electrochemical Impendence Spectroscopy curves.
The quantification of the transport limitations is done using analysis by the methods discussed in below. So we need the experimental data varying the operating conditions like Relative Humidity, Pressure to extract the parameters discussed before by fitting the simulated and the experimental curves. We will use the electrochemical characterization in different operating conditions. The polarization or the I-V curves that give the performance of the fuel cell as the stationary response. The electrochemical impedance spectroscopy is used to study the dynamic behavior by varying the frequency. Finally, the limiting current analysis studies the stationary response of the cell at maximum current density, this is used to see the effects if the parameters that are discussed above on the oxygen transport resistance.

1. Polarization Curve:
   The fitting of the polarization curve is done for the low current density (<0.2A/cm^2). At the low current density it could be assumed that the losses are mainly due to the kinetic limitations of the Oxygen Reduction Reaction and losses from the transport limitations can be considered negligible. The input parameters to the model are values that are known after the characterization, these are discussed in detail in the later section, and the list of parameters in the table 4. By fitting of the polarization curve, we extracted the electrochemical parameters of the oxygen reduction reaction.
   Adjusting for the crossover current at very low current densities (<0.02 A/cm^2), we fitted the crossover part of the polarization curve. The hydrogen crossover current mainly depends on the permeability of hydrogen in the membrane. The parameters controlling the permeability of hydrogen in the membrane can be extracted after the fitting.

2. Electrochemical Impendence Spectroscopy
   The electrochemical parameters that are extracted from the polarization curve were used here as the starting input parameters. The first step is the fitting of the high frequency ohmic resistance.
   For the fitting of the ohmic resistance we used the parameters governing the ionic conductivity of the membrane, at the high frequency part of the spectra. The conductivity law of the membrane could be extracted from the fitted parameters.
   The effect of change of many parameters like tortuosity of Nafion ionomer can be analyzed. The effect on the shape of the EIS curve of these parameters are noted to understand the physics of lumped phenomenon happening in the Membrane Electrode Assembly.

3. Limiting Current Analysis
   Limiting current in PEMFC is the maximum current that can be produced by the cell as the concentration of oxygen on the surface of the electrode approaches to zero. It is the maximum current that could be delivered by the electrode, and at the limiting current operation the concentration of the reactant on the surface of the electrode approaches to zero. At these conditions the effect of the electrokinetic parameters are negligible.
   The limiting current measurements can be used to separate the oxygen transport resistance into component parts of pressure dependent and independent components. In

this case we fit the parameters that affect the oxygen transport that the tortuosity of the GDL and MPL and the diffusion coefficient of oxygen.
By varying the pressure, the transport resistance is separated into a pressure-dependent component (intermolecular gas diffusion) and a pressure-independent component (Knudsen diffusion or transport through ionomer/liquid water layers) by studying the slope and intercept of the curve.

3.1 Polarization Curve

3.1.1 Description

The polarization curve analysis is the most common type of testing method that used to study the fuel cells and similar electrochemical systems. It is an established and understood method and the results are easier to compare with the existing studies. Polarization curves plot the voltage against the corresponding current density. The curves can be obtained in the potentiostatic or galvanostatic mode, drawing a fixed current from the fuel cell and measuring the output voltage. There are three distinct regions of a fuel cell polarization curve:

• At low current densities, the cell potential drops as a result of the kinetic limitations of the oxygen reduction reaction.
• At moderate current densities, the cell potential decreases linearly
• At high current densities, the cell potential drop is not linear because of the transport limitations.

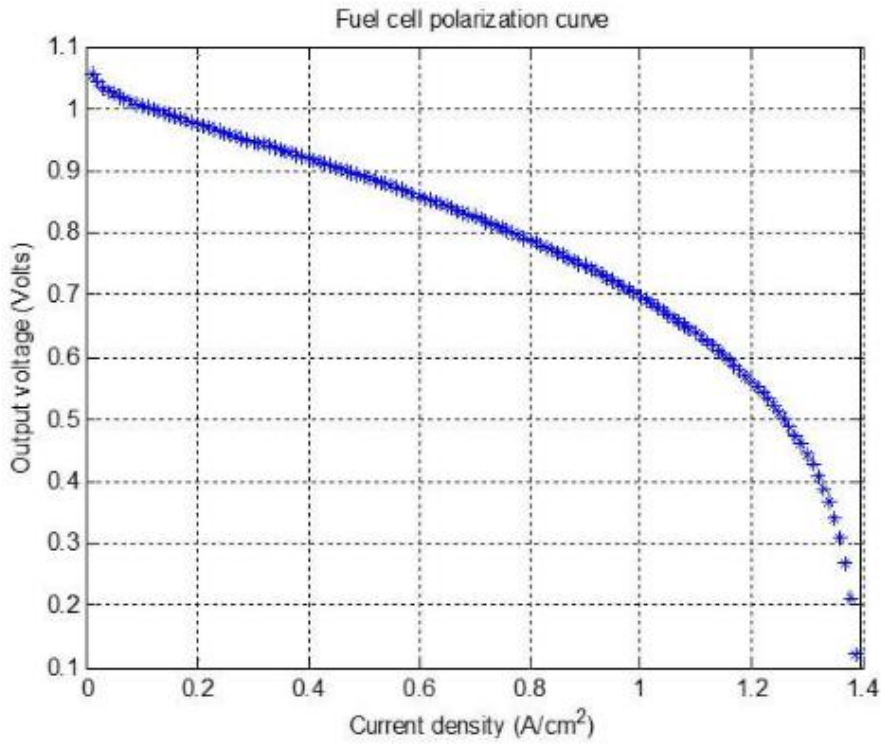

Figure 9: A generic Polarization curve [25]

In our case the change in the load is programmed to increase or decrease step wise. Reliable readings require a stable environment where temperature, pressure, humidity and flow rates are monitored and maintained at the desired values. In addition, the equilibrium has to be maintained while taking the readings at the particular condition.

3.1.2 Results and Discussions

There are certain parameters given as input to the model like the thickness of various domains, catalyst loading, pore radius, operating conditions. The values of the input parameters given in the tabkle 4, are known from the measurement and characterization methods to a good certainty. Given set of parameters are related to physical phenomena which are listed in the table below

Tableau 4: The list of input parameters and the phenomenon associated

Main Input parameters	**Phenomenon**
Tortuosity of GDL, MPL, CL	Transport of Oxygen
Tortuosity of ionomer in CL	Transport of Proton
Electronic conductivity of GDL, MPL,CL	Transport of electrons

The plots of the experimental data are straightforward. The simulated models on COMSOL and MATLAB gives the simulated plots for the same operating conditions and the setup as the experimental. The two can then be compared and fitted. The tuning of the parameters in the simulated model is done from the results of the fitting.
For the fitting of the polarization curves several parameters were considered. The parameters include the ones discussed in the table 5.

Tableau 5: The list of fitting parameters used in the simulation of Polarization curve

Fitting Parameters	**Description**
dHox0_c	The enthalpy of formation of activated complex in the cathode side
dSox0_c	The entropy of formation of activated complex in the cathode side
alpha_c	The charge transfer coefficient at the cathode
gamma_O2	The order of the reaction with respect to oxygen
gamma_H2O	The order of the reaction with respect to water
coef_Dh_naf_A_MB	Coefficient of Diffusion of Hydrogen in Membrane
coef_kappa_ld1_MB	Ionic conductivity of the membrane

These parameters were varied in various ranges of values, the simulation allows the change of the parameter these given ranges to check for minimization of the differences between the simulated

and experimental curves. We can see the example of one such run of simulation leading to the plotting of the simulated curve.

```
list_param={'dHox0_c','dSox0_c','alpha_c','gamma_O2','gamma_H2O'};
x_min     =[ -2.5e5     -1000      0.001      -200        -200    ];
x_max     =[ 2.5e5      1000       0.999      200         200    ];
```

Figure 10: An example of the simulation, the list of optimization parameters varied in the range

The first fitting of the polarization curve is done, with the adjustment of parameters, the enthalpy of formation of activated complex, alpha of the oxygen reduction reaction, the rate of the reaction with respect to oxygen and water. The values of the fitting parameters were obtained, we can see that the fitting at very low current densities (<0.02 A/cm^2) is not good. Improvements in the parameters at every step is noted and essential changes are made accordingly to improve the next runs.

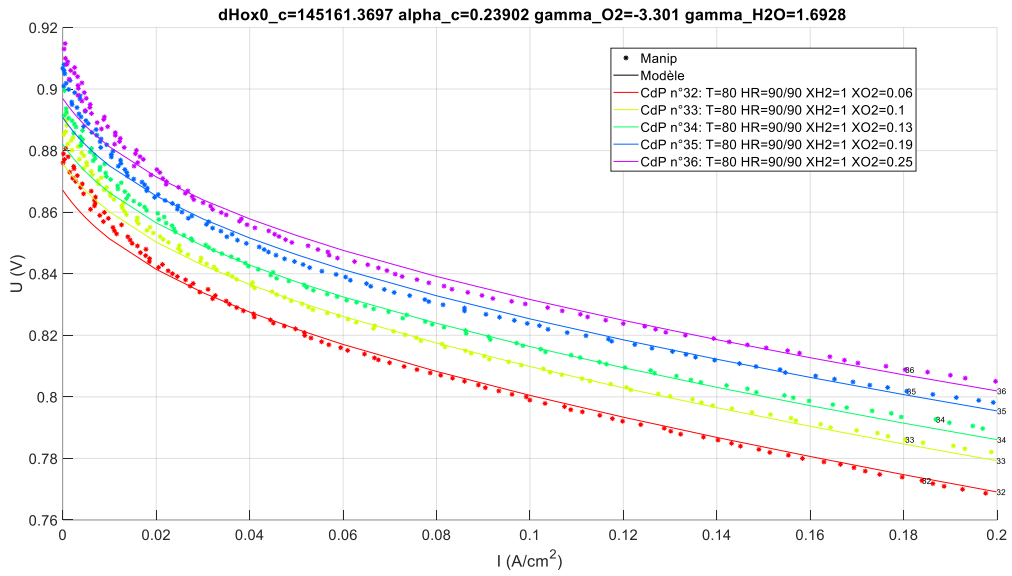

Figure 11: The fitting of the polarization curve at 80°C, 90 RH and different partial pressures of oxygen, without considering the permeation current parameters for I<0.2A/cm^2

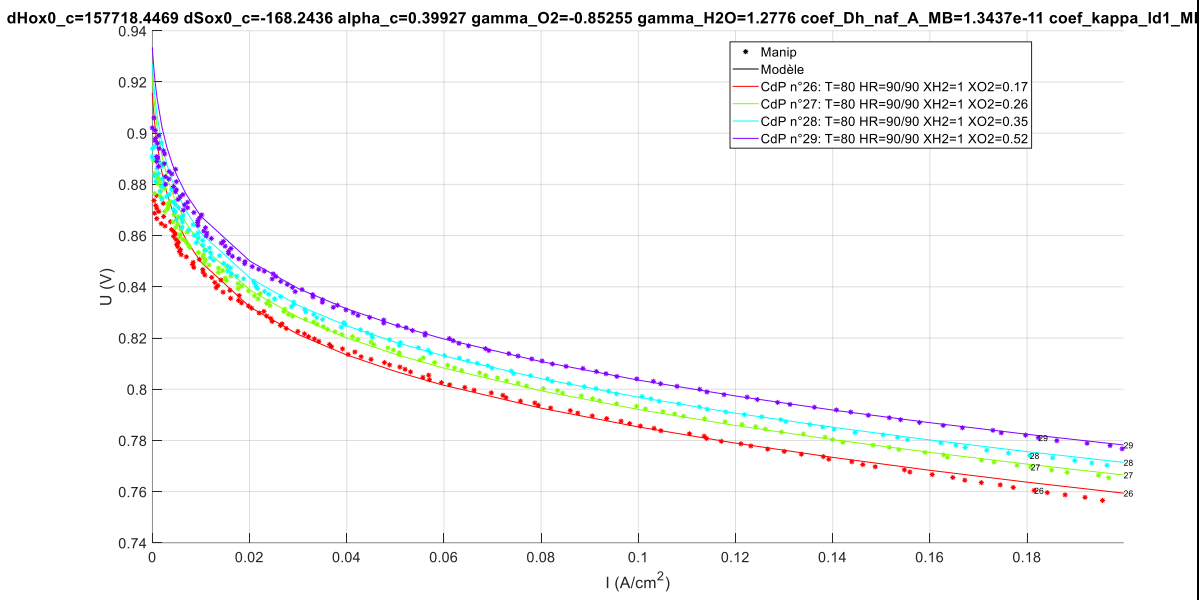

Figure 12: The fitting of the polarization curve at 80°C, 90 RH and different partial pressures of oxygen with the consideration of the parameters affecting the permeation current for I <0.2A/cm^2

It can be noticed in the figure 12 that the fitting is better at the lower current value (<0.02 A/cm^2), this is because of the inclusion of the parameters that control the permeation current, like the coefficient of diffusion of hydrogen in the membrane. The permeation current becomes significant at very low current densities as the cross over Hydrogen flux given in table 3 corresponds to a current density of a few mA/cm^2. These parameters of oxygen reduction reaction and permeation current are extracted and used as the input parameters to the Electrochemical Impedance Spectroscopy model.

3.2 Electrochemical Impendence Spectroscopy

3.2.1 Description

EIS method includes a sequence of sinusoidal potential signals with varying frequency, but similar amplitude is applied to an electrochemical system, in our case a PEM fuel cell. The impact signal is applied via a potentiostat or a galvanostat.

The theoretical modelling, experimental measurements, then fitting and tuning of parameters needs to be done for the optimization of PEMFC operation. Electrochemical Impedance Spectroscopy (EIS) is a powerful tool helpful in understanding of the PEMFC performance, trying to analyze the different elements of the complex system. A wide range of frequencies are used that are sensitive to both external and internal factors affecting the performance of PEMFC.

However, the interpretation of the EIS data can be ambiguous, and this is a major challenge in the extraction of useful information along with different experimental set up applied. The impendence model of the PEMFC is a good approximation, in these models the PEMFC is modelled as the equivalent circuit with electrical resistances, capacitances, and the impendences (for the electrical

wire connections, theoretically this must be affixed value) as shown in the figure 13. The equivalent electronic circuit describes an electrochemical interface between an electrode (electronic conductor), and the electrolyte (ion conductor), as a resistance in parallel with the capacitance. The former represents the resistance to an electrochemical faradic reaction at the interface and is called the charge transfer resistance. The latter is the capacitance due the accumulation of the charges at the interface between the electrode and electrolyte. An analytical expression for the impedance response of the assembly or part of the assembly like catalyst layer. The Rs is the ohmic resistance of the system. This type of simplified equivalent circuit model are helpful to understand the EIS response but they are oversimplify the complex physical interactions in the system, so these are not considered in this study.

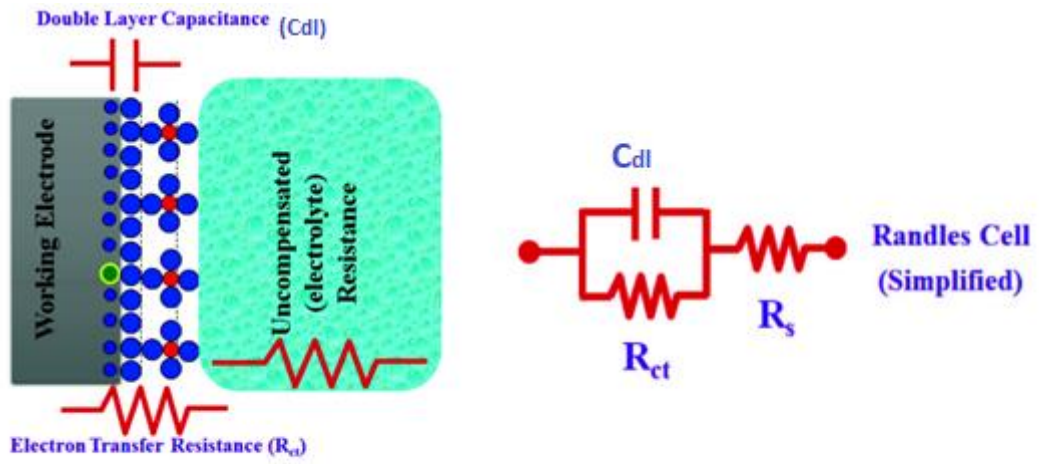

Figure 13: (left) The scheme of the electrochemical interface. (right) The simplified equivalent Randle's circuit model describing the impedance of the electrochemical interface (not used in this study)

We consider that the impedance is a dynamic response of the complex physics in each domain that has been described in the previous section.

The EIS method basically uses a wide range of frequencies to deconvolute different phenomenon occurring in different time scale at different frequencies. EIS is particularly sensitive to systems that have several impedance elements. Different components and processes within a cell operate on different time scales, they have different time constants (some phenomenon occurring at equal rates may have very similar time constants) and thus can be separated in the frequency domain[26].

The modeling could be done with electrochemical parameters as well. General observations that could be made are:

- In the very high frequency range, the information of purely ohmic (relatively fast processes) could be extracted. These processes mainly include the proton migration in the membrane, the electron movement in the GDL, CL, plates and the external circuit, and the anode side processes because of the fast kinetics of hydrogen oxidation reaction, hydrogen transport.

- In The high to intermediate frequency the information characterizing both kinetics of the cathode and proton migration could be extracted.
- For the lower frequency analysis, the information about the slower processes like water and oxygen transport phenomena could be extracted

3.2.2 Results and Discussions

1. **Fitting of the high frequency resistance**

The first step in the fitting of Electrochemical Impedance Spectroscopy curves is the determination of the high frequency ohmic resistance resistance (the ohmic resistance of the membrane is the major contributor to this resistance). The fitting of the parameters for the ionic conductivity of the membrane helps knowing the coefficients of the conductivity law of the membrane. Once we have the conductivity law of the membrane as shown in the equation 59, and we know the fraction of the water in the Nafion ionomer inside the membrane at the RH, so the conductivity of the Nafion in the membrane can be determined. The idea is to find the relationship between the proton resistance of the membrane and RH. The law of the conductivity K has to be adapted to have the correct proton membrane resistance for a given RH.

$$K = k_1 * (\lambda - k_3) * k_2 * \exp(k_T * \left(\frac{1}{T_0} - \frac{1}{T}\right)) \quad 32$$

Where, the k_1, k_2, k_3 are the parameters that effect the conductivity, k_T for the temperature dependence of the conducitivity and λ is the number of water molecules per sulphonic ion sites.

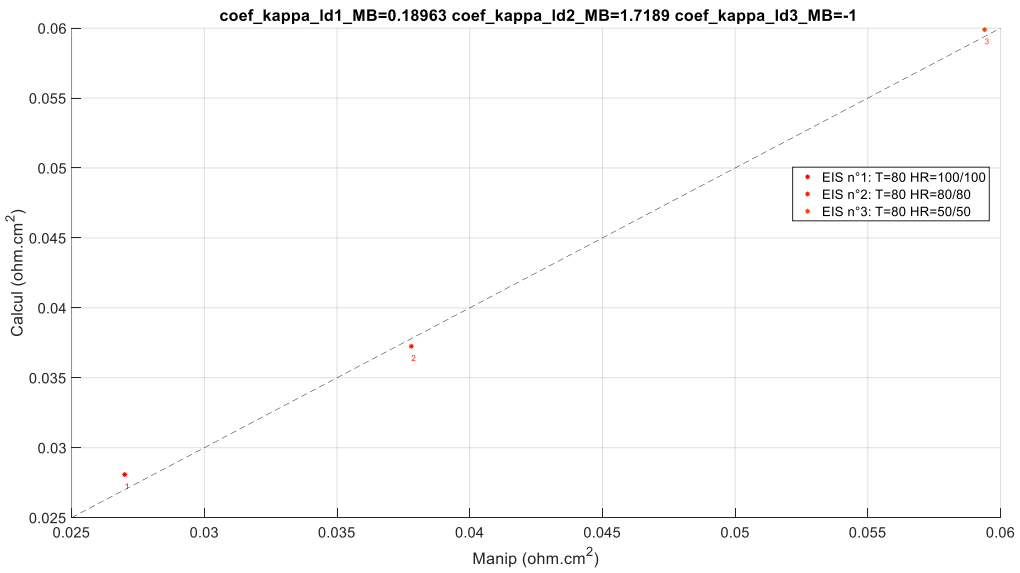

Figure 14: The fitting of the high frequency resistance curve at 80°C, 100, 80, 50 RH and 0.21 bar partial pressures of oxygen with the consideration of the parameters affecting the permeation current for $I < 0.2A/cm^2$

Given that, same ionomer is used in the catalyst layer (although the density of sulfonic acid group is not same, we can consider that the conductivity law is the same for the ionomer in the membrane and catalyst layer) and we know the fraction of the nafion ionomer in the catalyst layer. We can find the tortuosity of the Nafion in the catalyst layer by the fitting of protonic resistance of the catalyst layer considering that we know the relationship between the conductivity and the RH for the ionomer in the catalyst layer. This is important in estimation of transport properties of ionomer in the catalyst layer. This can be used to estimate the conductivity of the catalyst layer by equation 59, and further the resistance provided by the catalyst layer.
The next graph shown in the figure 15, gives the convergence of the parameters related to the total ohmic contribution (main part of this ohmic part comes from the membrane). We can notice that the value of the parameters becomes constant at the end of simulation. This is the condition of the convergence. This indicates a good fitting.

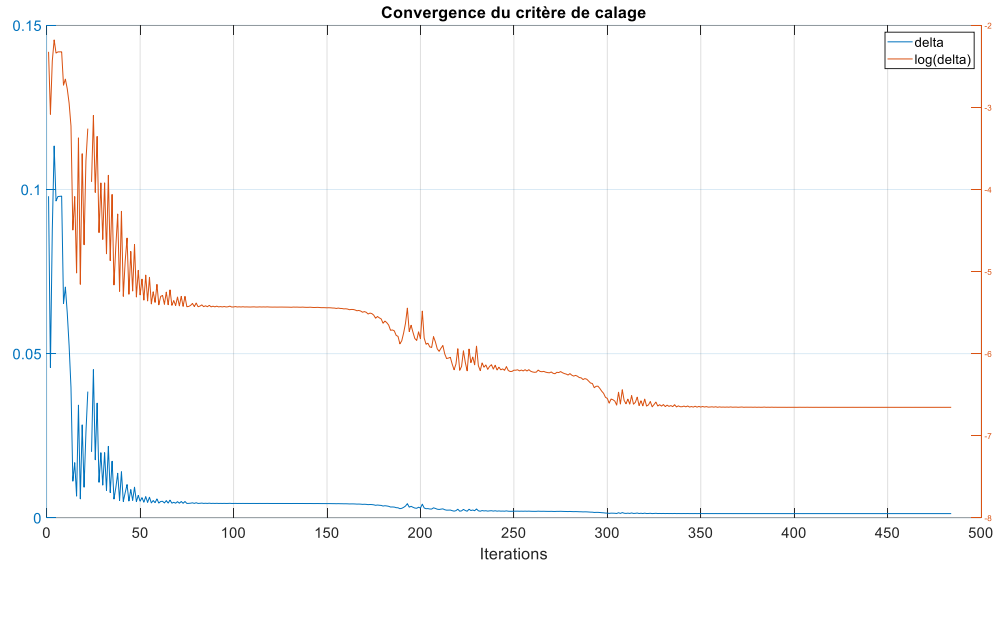

Figure 15: Convergence of the parameters in the fitting of high frequency resistance

2. Fitting of the EIS curve

Once we have the value of high frequency resistance, we can start fitting the curve of EIS. The electrochemical parameters of oxygen reduction reaction and the cross-over current extracted from the fitting of the polarization curve a low current density are used as input to the simulated EIS generation model.
The EIS experimental curves are plotted in a straightforward manner from the experimental readings obtained from the differential cells. The simulated models on COMSOL and MATLAB gives the simulated plots for the same operating conditions and the setup as the experimental. The two can then be compared and fitted.
Several simulations were done to identify the parameters that effect the shape and behavior of the simulated EIS curves. The parameters include

Tableau 6: The list of modelling parameters for the EIS curve simulation

Modelling parameters	**Description**
dHox0_c	The enthalpy of formation of activated complex in the cathode side
dHox0_a	The enthalpy of formation of activated complex in the anode side
sigma_CL_c	The electronic conductivity of the catalyst layer in cathode side
coef_Do_naf_A_CL	The coefficient of diffusion of oxygen in the Nafion
gamma_O2 Rp_dry_CL_c	Order of the reaction wrt oxygen Pore radius in the catalyst layer of cathode
coef_Dh_naf_A_MB	The coefficient of diffusion of hydrogen in membrane
Cdl_c	The double layer capacitance on the cathode side
tor_CL_c	The tortuosity of the catalyst layer in the cathode side
alpha_c	The charge transfer coefficient at the cathode
I_base	The base current of analysis
tor_naf_CL_c	The tortuosity of the nafion ionomer

The table 6 shows the list of the parameters that were tested for the shape of the EIS curve. The main parameters that affected the shape of the curve are limited. The following table 8 summarizes the effect of each parameter on the shape of the curve.
We start the fitting of the EIS curves, use various parameters to check the sensitivity of the curves towards these parameters. Here in Figure 16, 17 we can see that the parameter is tortuosity of nafion ionomer in the catalyst layer

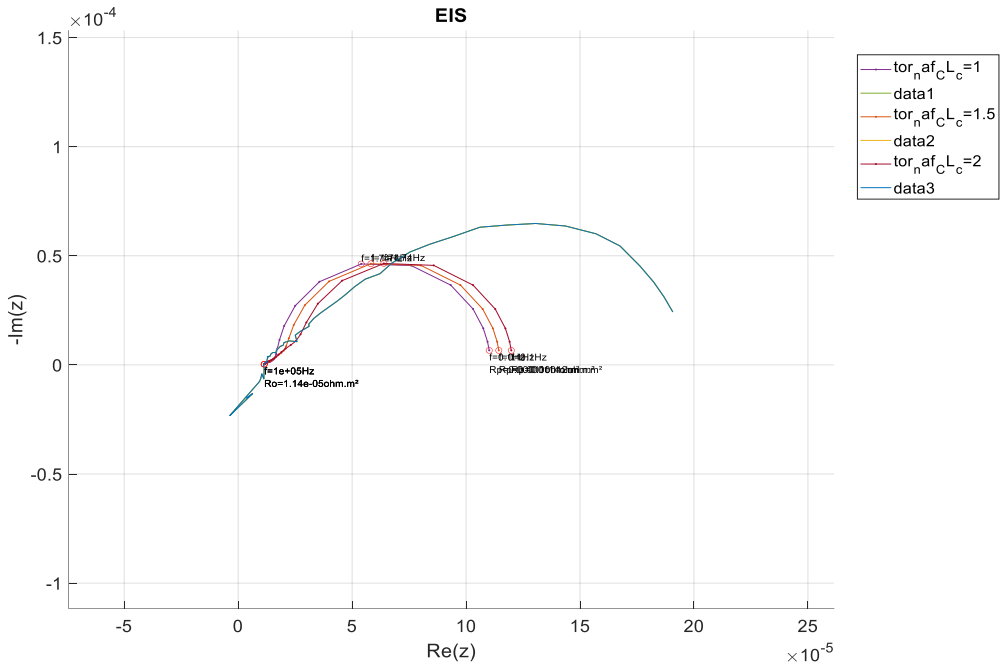

Figure 16: The simultaneous plot of experimental and simulated at 80°C, 50 RH and 0.21 bar partial pressures of oxygen, modelling parameter is the Tortuosity of Nafion at RH 50 at 0.2 A/cm^2

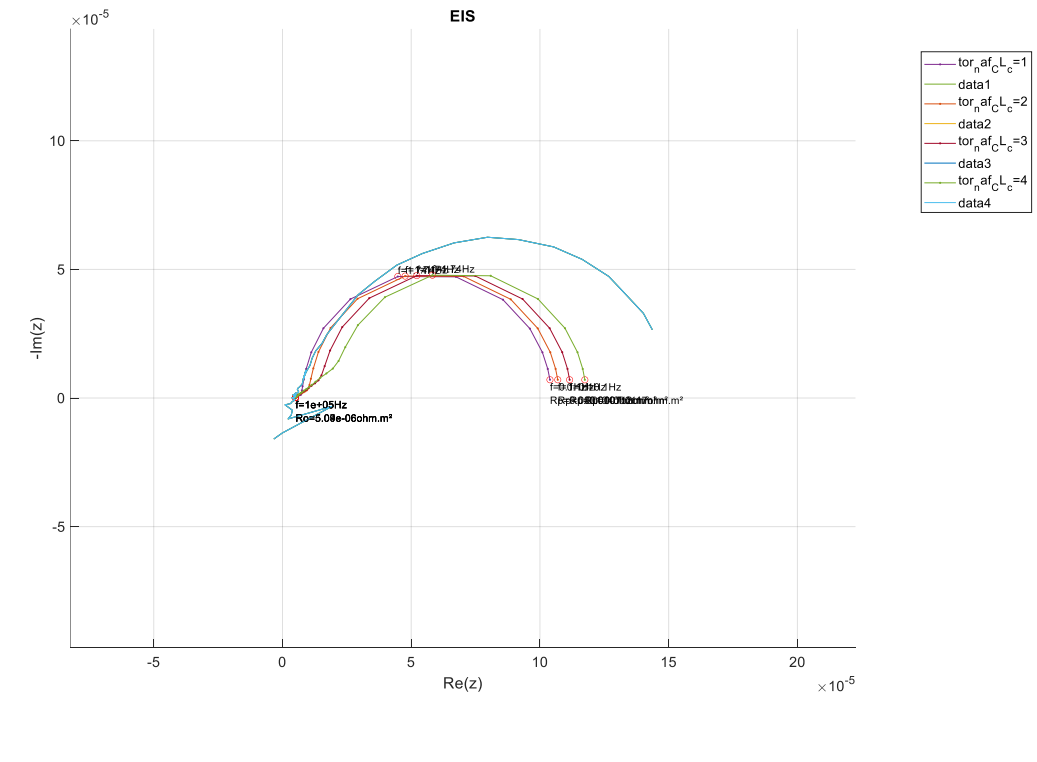

Figure 17: The simultaneous plot of experimental and simulated at 80°C, 50 RH and 0.21 bar partial pressures of oxygen, modelling parameter is the Tortuosity of Nafion at RH 90 at 0.2 A/cm^2

At the first site of the simulations the differences between the simulated and the experimental curves are quite evident. The above two plots in the figure 16 and 17 are at similar conditions with the difference in the levels of relative humidity. The first at 50 RH and the second at 90 RH. The high frequency part of the spectrum consists of the 45 degree line that is the characteristic of the proton migration resistance in the ionomer of the catalyst layer. For the higher value of the protonic resistance R_p, the elongated spectra are shifted to the right by $R_p/3$[26]

The next set of simulations were done to see what values of the tortuosity actually fit the experimental curve, the values were unrealistically high, good fitting is obtained at tortuosity 10. This value is too high, indicating very high charge transfer resistance.

We can see in the plot in figure 18 that the plot become wider in circumference as the tortuosity indicating the increase in the charge transfer resistance. Although these values of tortuosity are unrealistic they give us an idea about the charge transfer resistance is much more than accounted for in the model, indicating some missing physics or parasitic reactions of the oxidation of Platinum.

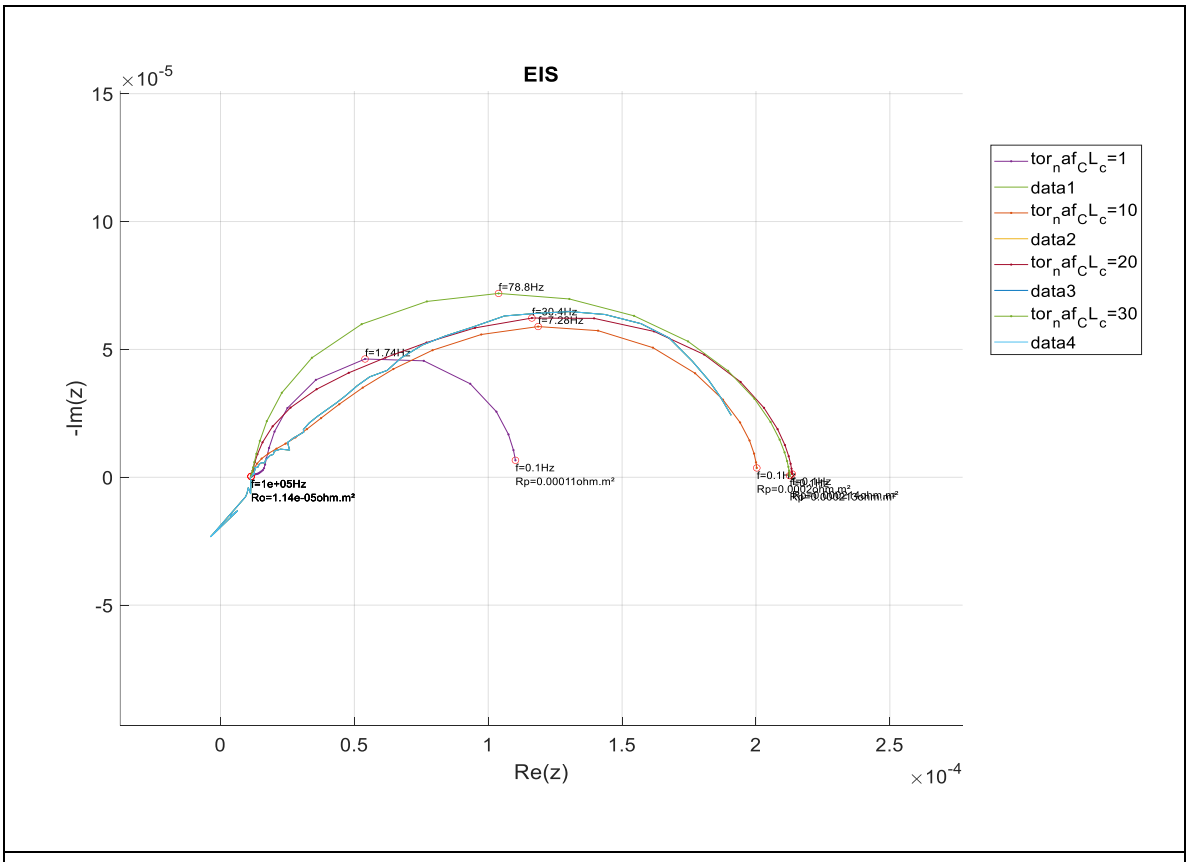

Figure 18: *The simultaneous plot of experimental and simulated at 80°C, 50 RH and 0.21 bar partial pressures of oxygen modelling parameter is the Tortuosity of Nafion (unrealistically high values) at* 20 mA/cm^2

We were also curious about the active surface area, if $1.8cm^2$ is a correct value. The actual area might be a bit larger, making the current density smaller than what we have. This maybe because a part of the area surrounding the gas flow field could produce some current because gas can have access, the GDL being slightly larger than the active area. There is an uncertainty in the actual active surface area.

So, we plotted I_base i.e. the current density as a parameter and the variation can be seen in Figure 19.

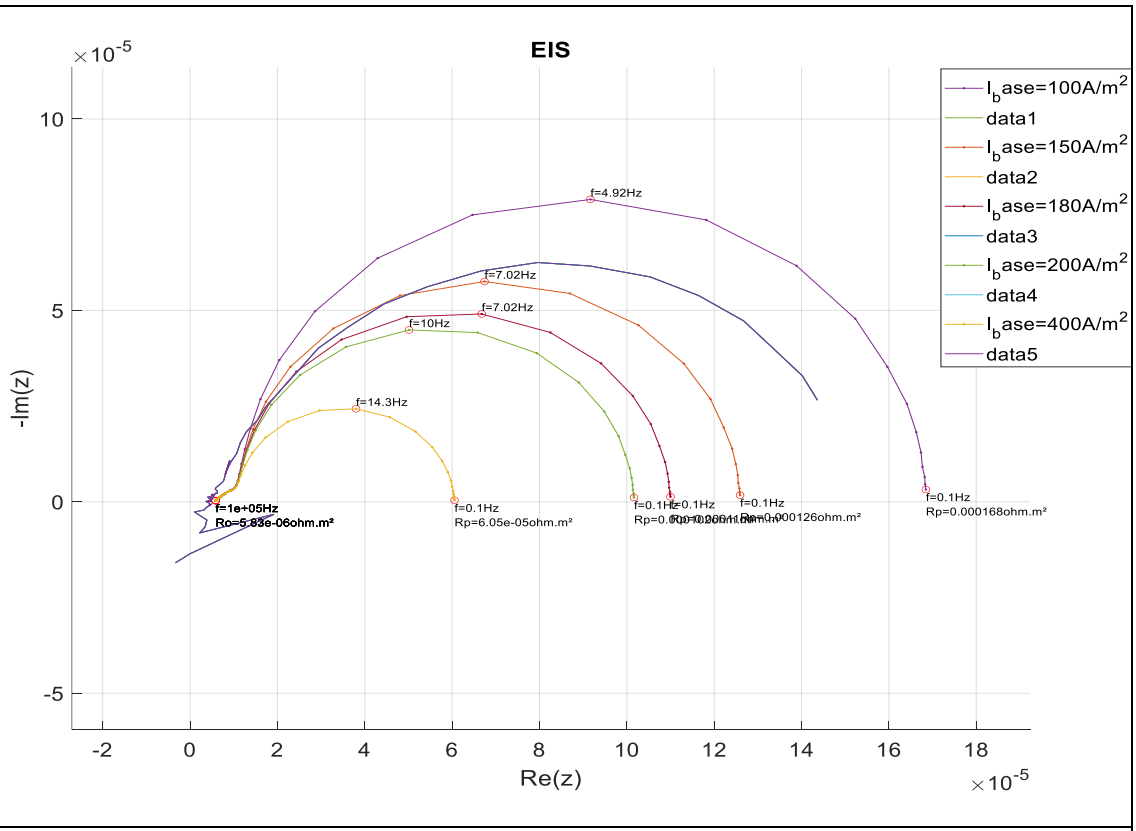

Figure 19: The simultaneous plot of experimental and simulated EIS at Low current density 90 RH , modelling parameter is I base

Several reasons for this difference in the shape could be:

1. During the experiment, the cell has been disassembled and reassembled, there might be problem of the compression of the GDL, leading to the issue of the contact resistance.
2. The model doesn't take into account the heterogeneities at the rib-channel scale.
3. The simplification of the reaction mechanism to a single step is not valid, the actual reaction is a multi-step mechanism. There are studies available on the double Tafel slope, arising from the complex reaction mechanism [9].

4. The underestimation of the base current density value, as the actual active area ($\sim 2.0 cm^2$)maybe higher than the value considered ($1.8 cm^2$)
5. The effect of gradient of concentration in the channel has not been considered in the current 1 D model.
6. Ignoring the additional mass transport limitation by the formation of water at the cathode at higher RH.

3.3 Limiting Current Analysis

3.3.1 Description

Limiting Current Analysis, LCA is an efficient method in determining the oxygen transport resistance in PEM fuel cells [27]. Here I will use a numerical model that allows good coupling with electrochemistry and other transport phenomena. The total transport resistance R_T
The components of the transport resistance can be separated into

1. Pressure dependent terms: These are the contributions from the large pores (>10 nm, GDL). These include the intermolecular diffusion.
2. Pressure independent terms: These are the contributions from the small pores (<10 nm, MPL, CL). The phenomenon include Knudsen diffusion or transport through hydrated ionomer in the CL or the liquid water layers [28].

This separation into the components can be done by the variation of the pressure.
The total oxygen transport resistance in the cell can be quantified as the ratio of the change in the concentration of oxygen from the channel inlet to the cathode electrode and the average normal molar flux of oxygen at the cathode.

$$R_T = \frac{\Delta c}{N_o} \tag{60}$$

The average molar flux N_o can be replaced by the simple Faraday's law and then the equation becomes

$$R_T = 4F\frac{\Delta c}{i} \tag{61}$$

Where Δc is the change in the concentration from the inlet of the channel to the electrode, but as we are in the limiting current operation the oxygen concentration at the electrode is zero, so Δc, is eaqual to the inlet concentration c_o.
The total resistance can be written as

$$R_T = 4F\frac{c_o}{i} \tag{33}$$

The inlet concentration depends on the dry mole fraction of oxygen

$$c_o = \frac{p - p_w}{RT} x_0^{dry-in} \tag{63}$$

Replacing the values and simplifying,

$$R_T = \frac{4Fx_0^{dry-in}}{i_{lim}} \frac{p - p_w}{RT} \quad 64$$

Components of the Transport Limitations
In this study we are aiming to identify the pressure dependent and independent components of the total transport resistance

$$R_T = R_P + R_{NP} \quad 34$$

In the real case it is complex to analyze the effects separately, as the different sources of the diffusion might not be in the simple series combination. MPL has different type of pore sizes and geometries.
In general, we can say that intermolecular diffusion may dominate in the larger pores, and Knudsen the smaller ones.
The three of the major components that contribute to the total oxygen transport resistance are:

a. The Flow Channels
b. The Diffusion Membrane (GDL)
c. The Microporous Layer

We will describe a simple analytical model that is often described in the literature in order to illustrate the oxygen transport limitations and help to understand .So, we can say that

$$R_T = R_{ch} + R_{DM} + R_{MPL} + R_{other} \quad 66$$

R_{other} represents all other sources of oxygen transport resistance in the cell. The basic geometry of atypical PEMFC has seven layers: two gas channels, two diffusion media and two catalyst layers and the electrolyte membrane. The total oxygen transport resistance can be expressed as [29]

$$R_T = R_{ch} + R_{DM} + R_{MPL} + R_{CL,gas} + R_{CL,ion} \quad 635$$

where,
R_{DM}, is the oxygen transport resistance in the Diffusion Membrane
$R_{CL,gas}$, is the oxygen transport resistance in the pores of Catalyst Layer
$R_{CL,ion}$, is the transport resistance of oxygen through the ionomer film

$$R_{DM} = \frac{h_{DM}}{D_{DM,O_2}^{eff}} \propto \frac{1}{D_{O_2:mix}} \quad 36$$

Where, h_{DM} is the thickness pf DM and D_{DM,O_2}^{eff} is the effective molecular diffusivity

$$R_{CL,gas} = \frac{h_{CL}^{eff}}{D_{CL,O_2}^{eff}} \propto \frac{h_{CL}^{eff}}{D_{knud,O_2}} \quad 69$$

Where, $h_{CL}^{eff} = h_{CL}/3$, consider the uniformly distributed transmission-line model

$$R_{CL,ion} = \frac{\delta_{ion}^{eff} H_{ion,O_2}}{A_{ion}^{eff} D_{ion,O_2} RT} \propto \frac{\delta_{CL}^{eff}}{\Psi_{ion,O_2} T\, A_{ion}^{eff}} \quad 70$$

Where, δ_{ion}^{eff} is the effective ionomer area for oxygen permeation and Ψ_{ion,O_2} is the oxygen permeation coefficient and

$$\Psi_{ion,O_2} = \frac{D_{ion,A}}{H_{ion,A}} = 3.27 \times 10^{-15} \exp[1.28(RH)] \times \exp\left[\frac{17200}{R}\left(\frac{1}{323.15} - \frac{1}{T}\right)\right] mols^{-1}m^{-1}P_a^{-1} \quad 71$$

The transport resistance can be expressed as

$$R = \frac{h}{D_A^{eff}} \quad 72$$

D_A^{eff} , is the effective diffusivity has to be adjusted according to the porosity, ε_o, and tortuosity, τ of the porous media

$$D_A^{eff} = \frac{\varepsilon_o D_A}{\tau} \quad 73$$

And, the Diffusion Coefficient is estimated as

$$\frac{1}{D_A} = \frac{1}{D_{Knud,A}} + \frac{1}{D_{A:mix}} \quad 74$$

The Knudsen diffusion can be evaluated from the following expression[30]

$$D_{Knud,A} = \frac{2r_{knud}}{3}\sqrt{\frac{8RT}{\pi M_A}} \quad 75$$

And the molecular diffusion coefficient is calculated as

$$D_{A:mix} = \left(\sum_{\substack{j=1 \\ j \neq A}}^{N_c} \frac{x_j}{D_{A:j}} \right)^{-1} \quad 76$$

For two components

$$D_{A:B} = 0.001 \frac{T^{1.75}}{P\left(v_A^{\frac{1}{3}} + v_B^{\frac{1}{3}}\right)^2} \sqrt{\frac{1}{M_A} + \frac{1}{M_B}} \quad 77$$

To evaluate the oxygen transport resistance of each diffusion mechanism, the sensitivity of different diffusion resistances towards different operating conditions can be checked using the relationships [29]. A, B are the reaction and balance gas respectively.

Tableau 7: The sensitivity parameters of different diffusion resistance towards different operating conditions

	Molecular Diffusion Resistance	Knudsen Diffusion Resistance	Ionomer Permeation Resistance
Gas Pressure $[P]$	P	1	1
Balance gas $[M_B]$ (N_2/He)	$\frac{\left(v_A^{\frac{1}{3}} + v_B^{\frac{1}{3}}\right)^2}{M_{AB}^{1/2}}$ 3.5	1	1
Reaction gas $[M_A]$ (O_2/H_2)	$\frac{\left(v_A^{\frac{1}{3}} + v_B^{\frac{1}{3}}\right)^2}{M_{AB}^{1/2}}$ 3.7	$\sqrt{M_A}$ 4.0	$f(M_A)$ 2.2
Temperature $[T]$ 40/80°C	$T^{-1.75}$ 1.2	$T^{-0.5}$ 1.1	$T^{-1}e^{-17200/RT}$ 2.4
Humidity $[RH]$	1	1	$e^{-1.28[RT]}$
Thickness $[h]$	h_{DM}	h_{CL}^{eff}	δ_{ion}^{eff}

Where, $M_{AB}^{1/2} = \sqrt{\frac{1}{M_A} + \frac{1}{M_B}}$

3.3.2 Results and Discussions

As we can see in the plot of that the limiting current increases with the increasing total pressure as expected. We tried to fit the experimental and simulated plots of the limiting current vs the dry mole fraction of oxygen. The parameters that are changed are the tortuosity of GDL and MPL. It can be seen in that change in the values of tortuosities of GDL and MPL changes the slope. We

got the fitted values of the tortuosity of the GDL and MPL as 2.41 and 1.65 respectively. It can be stated that this is not a unique set of values that would satisfy the fitting, a number of values of sets of GDL and MPL that would satisfy the condition. The set of the values is one of the viable solutions. There are other set of values that might satisfy the condition well. The sensitivity is higher for the tortuosity of GDL, as the change in the value of tortuosity of GDL has a more pronounced effect on the slope of the curve compared to the tortuosity of MPL.

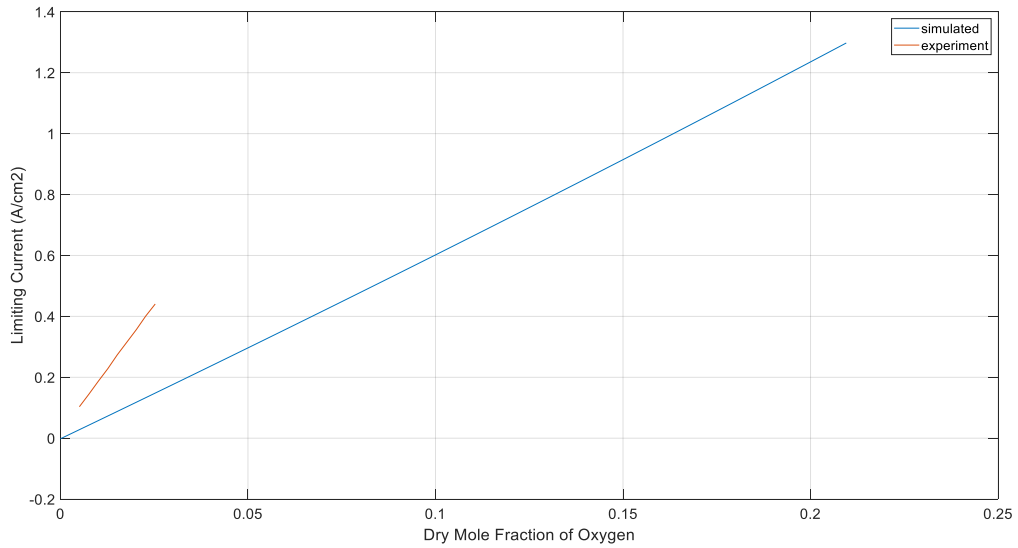

Figure 20: The variation of the Limiting current with the dry mole fraction of oxygen changing the tortuosity of GDL=5 and MPL=2

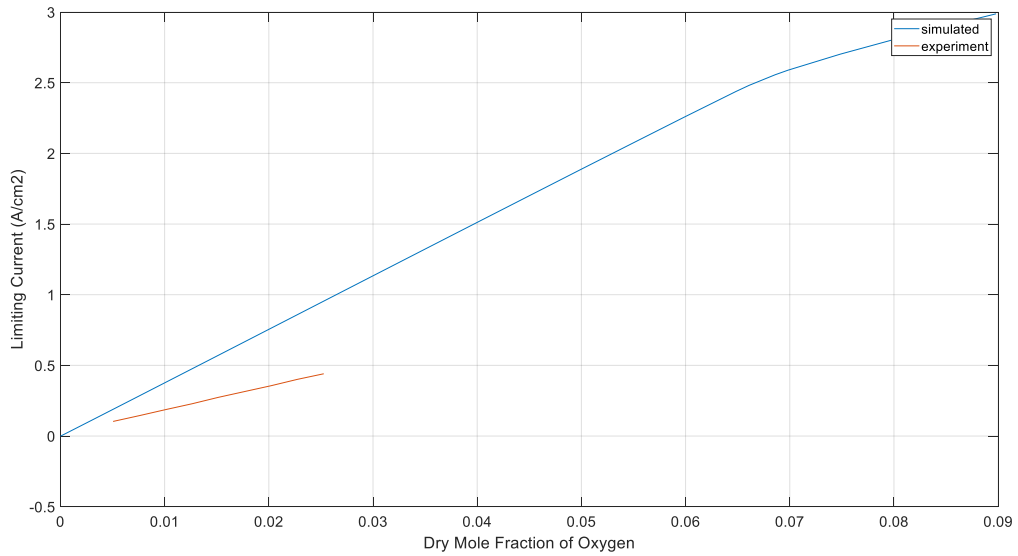

Figure 21: The variation of the Limiting current with the dry mole fraction of oxygen changing the tortuosity of GDL=1 and MPL=2

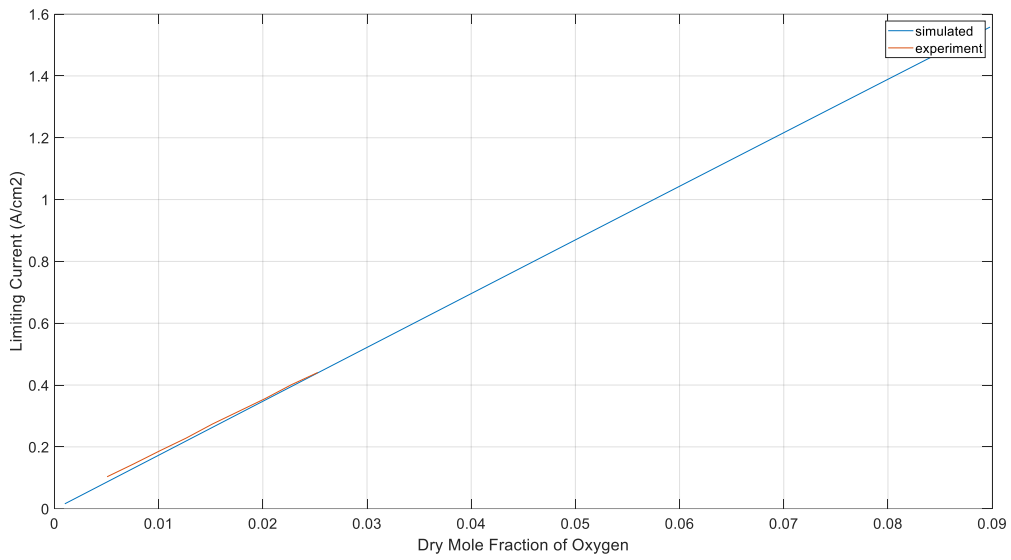

Figure 22: The variation of the Limiting current with the dry mole fraction of oxygen changing the tortuosity of GDL=2.41 and MPL=1.65

At a given dry mole fraction of oxygen, the limiting current increases with the increase in total pressure. The saturated values at higher mole fraction indicate that it is no longer a condition of limiting current, i.e. of the oxygen starvation is no longer achieved. The limitations comes from the transport in the model used in COMSOL. At higher mole fraction of oxygen, the limiting current conditions is no longer true. This can be seen in the figure 23

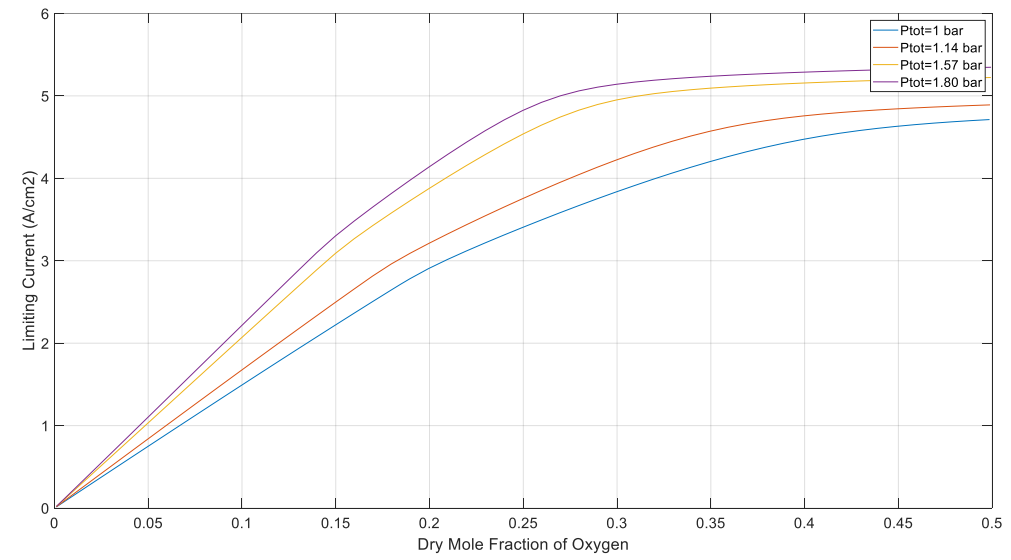

Figure 23: The variation of the Limiting current with the dry mole fraction of oxygen at different total pressure

The transport resistance increases with the increase in the tortuosity of the gas diffusion layer at a given pressure as shown in the plot in figure 24. As the tortuosity is the ratio of the actual flow path to the shortest distance between the ends of the flow path, so increasing tortuosity leads to increase the total transport resistance of oxygen.

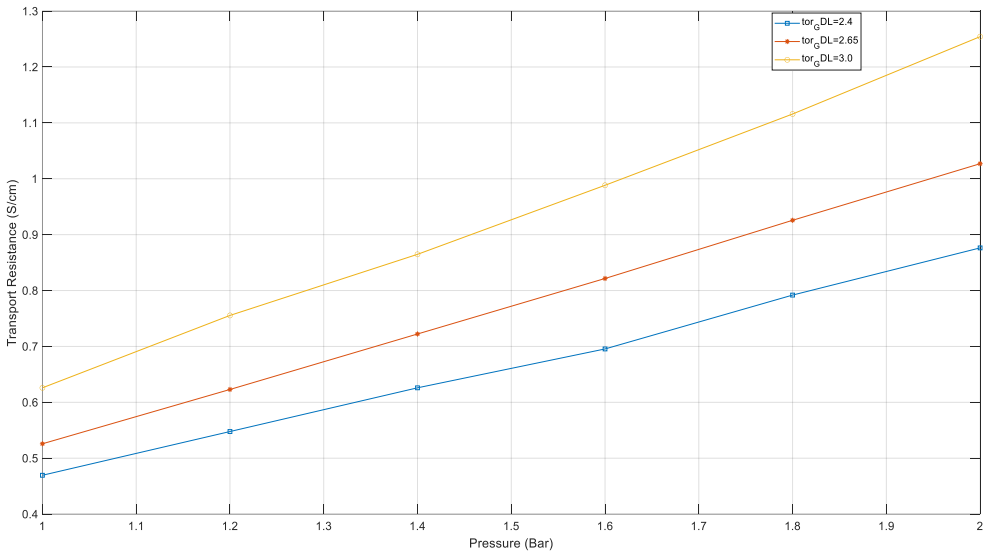

Figure 24: The variation of the total transport resistance with the pressure at different tortuosity of GDL

The transport resistance increases with the increase in the tortuosity of the microporous layer at a given pressure as seen in the figure 25.

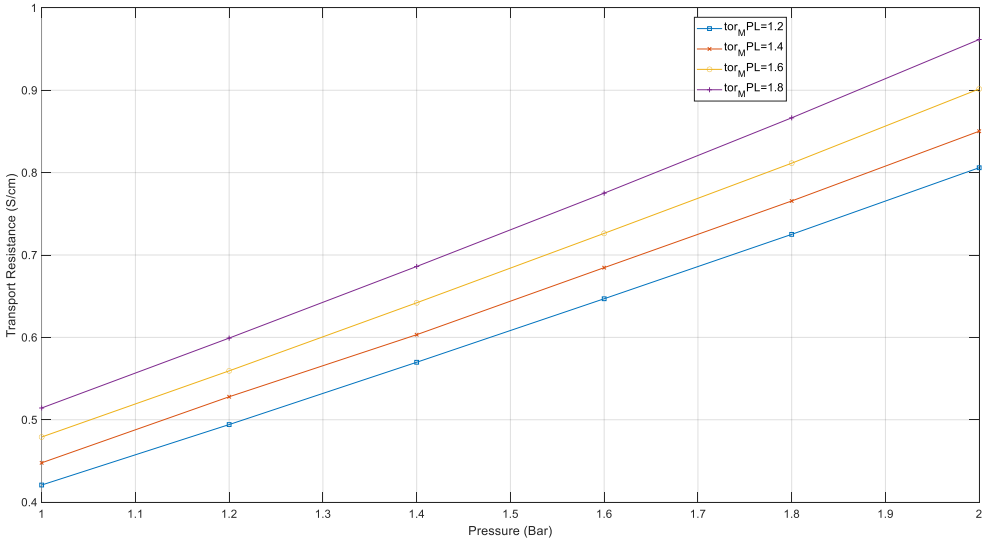

Figure 25: The variation of the total transport resistance with pressure at different tortuosity of MPL

We also studied the variation of the slope and intercepts of the above curves. The results were interesting to observe. The Pressure dependent and independent parts of the total resistance are closely related to the intercept and slope of the graph of the Total resistance and Pressure. The slope of the curve gives information about the pressure independent part and slope gives the idea about the dependent part as shown in the figures 26 and 27.
The slope of the curve of Transport resistance against the tortuosity of the GDL increases with the increase in the tortuosity, as shown in figure 26.

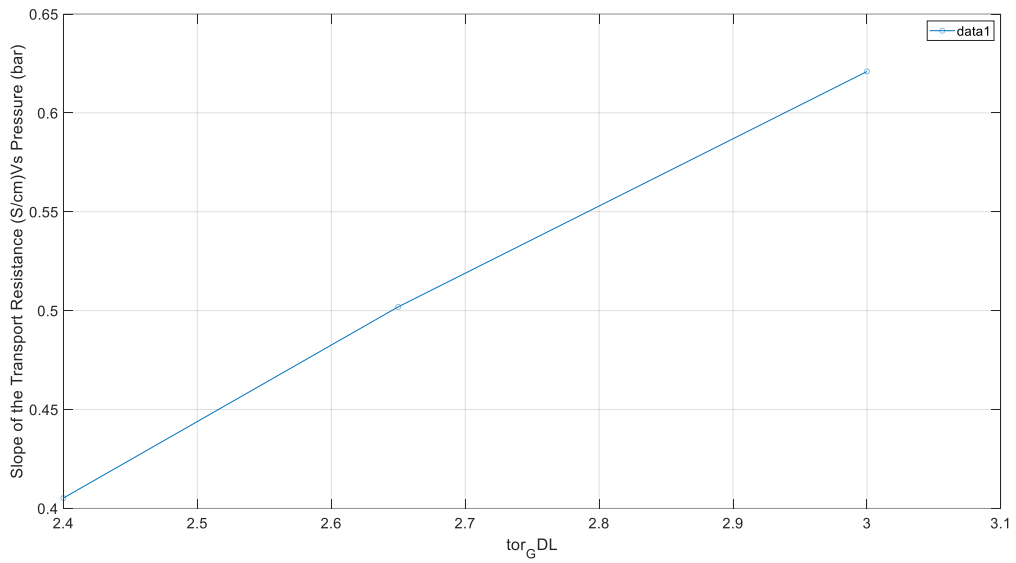

Figure 26: The variation of the slope of the transport resistance against pressure with the tortuosity of GDL

The intercept curve of Transport resistance against the tortuosity of the GDL decreases with the increase in the tortuosity of GDL as shown in Figure 27.

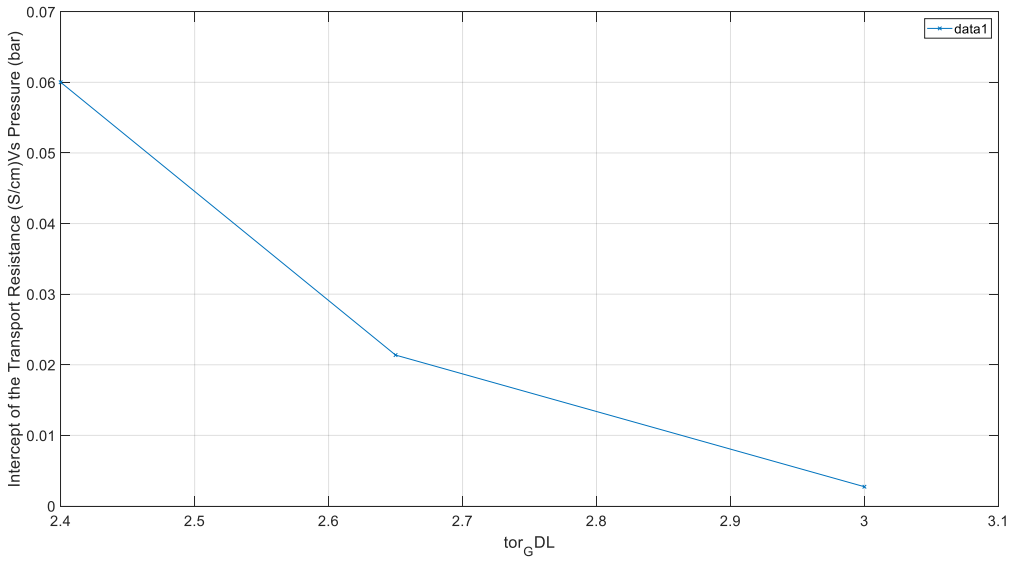

Figure 27: The variation of the intercept of the transport resistance against pressure with the tortuosity of GDL

The slope of the curve of Transport resistance against the tortuosity of the MPL, increases with the increase in the tortuosity of MPL, as shown in figure 28, 29

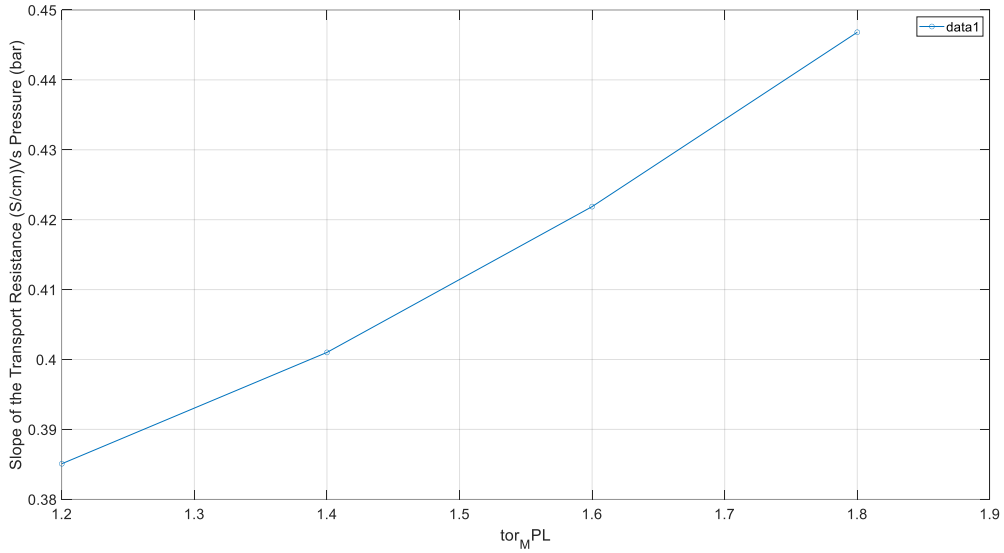

Figure 28: The variation of the slope of the transport resistance against pressure with the tortuosity of MPL

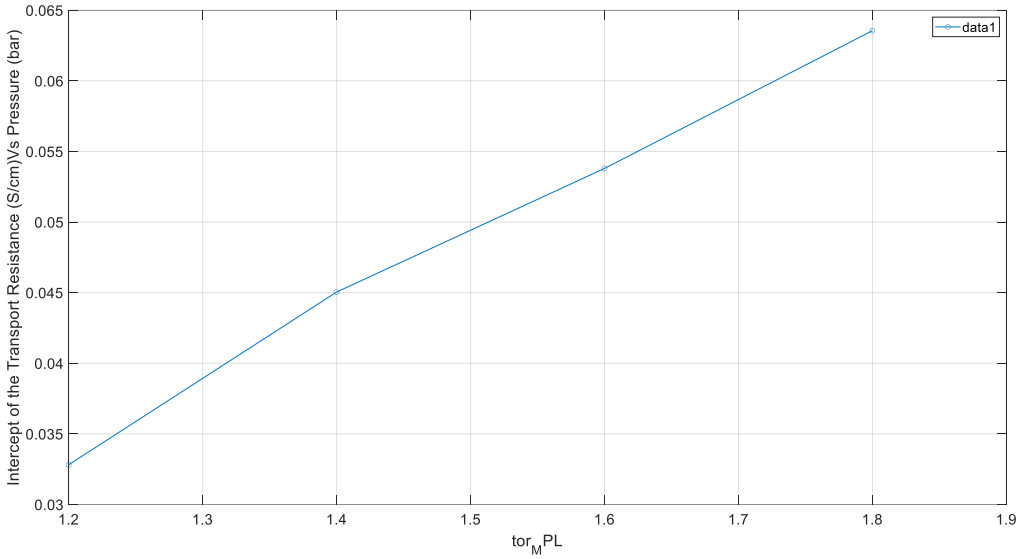

Figure 29: The variation of the intercept of the transport resistance against pressure with the tortuosity of MPL

The intercept of the curve of Transport resistance against the tortuosity of the MPL, increases with the increase in the tortuosity of MPL as shown in figure 29.

4. CONCLUSIONS

The fitting of the Polarization is done, we have the values of the electrochemical parameters related to the oxygen reduction reaction. These parameters were input to the Electrochemical Impendence Spectroscopy simulations.
Sensitivity analysis for various parameters have been done shape of Electrochemical Impedance Spectroscopy curves at low (<0.2A/cm^2) and high current density (till 2-3A/cm^2). Not all parameters effect the shape of the EIS curve. The effect of some parameters are prominent than the others. The table given below summarizes the effect of each parameter that has been changed for the simulated EIS spectra.

Tableau 8: The effect of various parameters on the shape of EIS

Modelling parameters	**Description**	**Effects on EIS**
dHox0_c	The enthalpy of formation of activated complex in the cathode side	No effect
dHox0_a	The enthalpy of formation of activated complex in the anode side	No effect
sigma_CL_c	The electronic conductivity of the catalyst layer in cathode side	No effect
coef_Do_naf_A_CL	The coefficient of diffusion of oxygen in the nafion	No effect
gamma_O2	Order of the reaction wrt oxygen	No effect
Rp_dry_CL_c	Pore radius in the Catalyst layer of cathode	No effect
alpha_a	The charge transfer coefficient at the anode	No effect
coef_Dh_naf_A_MB	The coefficient of diffusion of hydrogen in membrane	Slight effect, size of the arc decreases with higher values
Cdl_c	The double layer capacitance on the cathode side	No effect in shape, peak at different frequencies
tor_CL_c	The tortuosity of the catalyst layer in the cathode side	No effect at low values, slightly smaller arc can be seen at low values

alpha_c	The charge transfer coefficient at the cathode	The arc is small for small values (0.1, 0.2, 0.3)
I_base	The base current of analysis	The arc gets significantly bigger at lower base current, matches the experimental curve.
tor_naf_CL_c	The tortuosity of the nafion ionomer	The effect is small at small values of tortuosity of ionomer, pronounced effect at higher values. The arc is smaller for smaller values

We have seen the effect of various parameters on oxygen transport resistance through the Limiting current analysis. The limiting current is more sensitive to the tortuosity of GDL than MPL. The effect of total pressure on the limiting current have been studied. The effect of tortuosity of GDL and MPL on the transport resistance have also been studied, the slopes and intercepts of these graph have been seen. The transport resistance increases with the increase in the tortuosity of GDL and MPL. The slope of the plot of transport resistance vs tortuosity of GDL increases with the increase in the tortuosity while the intercept decreases with the increase in the tortuosity of GDL. The plot of transport resistance vs the tortuosity of MPL, both the slope and intercept of the plot increases with the increase in the tortuosity of MPL.

5. FURTHER DEVELOPMENTS

The current application of the model in 1D has several limitations as discussed above. The implementation of the 2D model can be a good step of improvement for the future studies especially for the Limiting Current Density Analysis. The concentration gradient along the channel has been ignored in the current 1D model. Application of Navier-Stokes in the channel while the implementation of the 2D model can be done, and further compared with the current results of 1D model so if there are any prominent differences, those can be noted.

An important aspect to investigate is the reason for the discrepancy between simulated and experimental Electrochemical Impedance Spectroscopy (EIS) data. The current model fails to account for certain physical phenomena, such as the multistep mechanism of Oxygen Reduction Reaction (ORR) and the possibility of parasitic reactions, such as the oxidation of Platinum. To bridge this gap, these missing mechanisms should be explored in future studies, enabling a more accurate representation of the system and, consequently, a better alignment between simulation and experimental results. The sensitivity analysis for various operating conditions on the oxygen transport resistance is an interesting area to explore for the future work.

6. REFERENCES

[1] "CEA Grenoble," *Wikipédia*. May 15, 2023. Accessed: Jul. 10, 2023. [Online]. Available: https://fr.wikipedia.org/w/index.php?title=CEA_Grenoble&oldid=204267117
[2] CEA, "Grenoble," *CEA/De la recherche à l'industrie*, Jun. 29, 2023. https://www.cea.fr/Pages/le-cea/les-centres-cea/grenoble.aspx (accessed Jul. 10, 2023).
[3] "De la recherche à l'industrie - Le CEA, acteur majeur de la recherche au service de l'Etat, de l'économie et des citoyens." https://www.cea.fr/ (accessed Jul. 10, 2023).
[4] O. Z. Sharaf and M. F. Orhan, "An overview of fuel cell technology: Fundamentals and applications," *Renew. Sustain. Energy Rev.*, vol. 32, pp. 810–853, Apr. 2014, doi: 10.1016/j.rser.2014.01.012.
[5] "- IEA." https://www.iea.org/publications/freepublications/publication/TechnologyRoadmapHydrogenandFuelCells.pdf (accessed Jul. 18, 2023).
[6] T. A. M. Suter *et al.*, "Engineering Catalyst Layers for Next-Generation Polymer Electrolyte Fuel Cells: A Review of Design, Materials, and Methods," *Adv. Energy Mater.*, vol. 11, no. 37, p. 2101025, 2021, doi: 10.1002/aenm.202101025.
[7] E. J. F. Dickinson and G. Hinds, "The Butler-Volmer Equation for Polymer Electrolyte Membrane Fuel Cell (PEMFC) Electrode Kinetics: A Critical Discussion," *J. Electrochem. Soc.*, vol. 166, no. 4, p. F221, Feb. 2019, doi: 10.1149/2.0361904jes.
[8] "Butler-Volmer Equation - an overview | ScienceDirect Topics." https://www.sciencedirect.com/topics/engineering/butler-volmer-equation (accessed Jul. 11, 2023).
[9] J. X. Wang, F. A. Uribe, T. E. Springer, J. Zhang, and R. R. Adzic, "Intrinsic kinetic equation for oxygen reduction reaction in acidic media: the double Tafel slope and fuel cell applications," *Faraday Discuss.*, vol. 140, no. 0, pp. 347–362, 2009, doi: 10.1039/B802218F.
[10] "17007_fuel_cell_system_cost_2017.pdf." Accessed: Jul. 10, 2023. [Online]. Available: https://www.hydrogen.energy.gov/pdfs/17007_fuel_cell_system_cost_2017.pdf
[11] A. Kongkanand and M. F. Mathias, "The Priority and Challenge of High-Power Performance of Low-Platinum Proton-Exchange Membrane Fuel Cells," *J. Phys. Chem. Lett.*, vol. 7, no. 7, pp. 1127–1137, Apr. 2016, doi: 10.1021/acs.jpclett.6b00216.
[12] Y. Shao, G. Yin, and Y. Gao, "Understanding and approaches for the durability issues of Pt-based catalysts for PEM fuel cell," *J. Power Sources*, vol. 171, no. 2, pp. 558–566, Sep. 2007, doi: 10.1016/j.jpowsour.2007.07.004.
[13] J. Wu *et al.*, "A review of PEM fuel cell durability: Degradation mechanisms and mitigation strategies," *J. Power Sources*, vol. 184, no. 1, pp. 104–119, Sep. 2008, doi: 10.1016/j.jpowsour.2008.06.006.
[14] R. Jinnouchi *et al.*, "The role of oxygen-permeable ionomer for polymer electrolyte fuel cells," *Nat. Commun.*, vol. 12, p. 4956, Aug. 2021, doi: 10.1038/s41467-021-25301-3.
[15] "Grant Agreement-875025-FURTHER-FC.pdf."
[16] T. Jahnke *et al.*, "Performance and degradation of Proton Exchange Membrane Fuel Cells: State of the art in modeling from atomistic to system scale," *J. Power Sources*, vol. 304, pp. 207–233, Feb. 2016, doi: 10.1016/j.jpowsour.2015.11.041.
[17] S. Mazumder and J. Cole, "Rigorous 3-D Mathematical Modeling of PEM Fuel Cells II. Model Predictions with Liquid Water Transport," *J. Electrochem. Soc.*, vol. 150, pp. A1510–A1517, Nov. 2003, doi: 10.1149/1.1615609.
[18] M. J. Lampinen and M. Fomino, "Analysis of Free Energy and Entropy Changes for Half-Cell Reactions," *J. Electrochem. Soc.*, vol. 140, no. 12, p. 3537, Dec. 1993, doi: 10.1149/1.2221123.
[19] "Henry's Law: Factors, Applications and Limitations." https://collegedunia.com/exams/henrys-law-chemistry-articleid-8538 (accessed Jul. 11, 2023).

[20] J. B. Young and B. Todd, "Modelling of multi-component gas flows in capillaries and porous solids," *Int. J. Heat Mass Transf.*, vol. 48, no. 25, pp. 5338–5353, Dec. 2005, doi: 10.1016/j.ijheatmasstransfer.2005.07.034.
[21] B. Randrianarizafy, P. Schott, M. Chandesris, M. Gerard, and Y. Bultel, "Design optimization of rib/channel patterns in a PEMFC through performance heterogeneities modelling," *Int. J. Hydrog. Energy*, vol. 43, no. 18, pp. 8907–8926, May 2018, doi: 10.1016/j.ijhydene.2018.03.036.
[22] F. Meier and G. Eigenberger, "Transport parameters for the modelling of water transport in ionomer membranes for PEM-fuel cells," *Electrochimica Acta*, vol. 49, no. 11, pp. 1731–1742, Apr. 2004, doi: 10.1016/j.electacta.2003.12.004.
[23] T. E. Springer, T. A. Zawodzinski, and S. Gottesfeld, "Polymer Electrolyte Fuel Cell Model," *J. Electrochem. Soc.*, vol. 138, no. 8, p. 2334, Aug. 1991, doi: 10.1149/1.2085971.
[24] G. Lin and T. Nguyen, "A Two-Dimensional Two-Phase Model of a PEM Fuel Cell," *J. Electrochem. Soc.*, vol. 153, pp. A372–A382, Feb. 2006, doi: 10.1149/1.2142267.
[25] P. H. Savasani, "Characteristics and Modeling of Pem Fuel Cell," *Int. J. Eng. Res.*, vol. 2, no. 9, 2013.
[26] T. Gaumont, G. Maranzana, O. Lottin, J. Dillet, L. Guétaz, and J. Pauchet, "In Operando and Local Estimation of the Effective Humidity of PEMFC Electrodes and Membranes," *J. Electrochem. Soc.*, vol. 164, pp. F1535–F1542, Nov. 2017, doi: 10.1149/2.0161714jes.
[27] M. V. Williams, E. Begg, L. Bonville, H. R. Kunz, and J. M. Fenton, "Characterization of Gas Diffusion Layers for PEMFC," *J. Electrochem. Soc.*, vol. 151, no. 8, p. A1173, Jun. 2004, doi: 10.1149/1.1764779.
[28] D. R. Baker, D. A. Caulk, K. C. Neyerlin, and M. W. Murphy, "Measurement of Oxygen Transport Resistance in PEM Fuel Cells by Limiting Current Methods," *J. Electrochem. Soc.*, vol. 156, no. 9, p. B991, Jun. 2009, doi: 10.1149/1.3152226.
[29] N. Nonoyama, S. Okazaki, A. Z. Weber, Y. Ikogi, and T. Yoshida, "Analysis of Oxygen-Transport Diffusion Resistance in Proton-Exchange-Membrane Fuel Cells," *J. Electrochem. Soc.*, vol. 158, no. 4, p. B416, Mar. 2011, doi: 10.1149/1.3546038.
[30] "Transport Phenomena, Revised 2nd Edition | Wiley," *Wiley.com*. https://www.wiley.com/en-gb/Transport+Phenomena%2C+Revised+2nd+Edition-p-9780470115398 (accessed Jul. 11, 2023).